Western Graduate&PostdoctoralStudies

Western University
Scholarship@Western

Electronic Thesis and Dissertation Repository

2-7-2020 2:30 PM

Analysis of Oxidatively Damaged Proteins by Mass Spectrometry

Vincent Saullo, *The University of Western Ontario*

Supervisor: Lars Konermann, *The University of Western Ontario*

A thesis submitted in partial fulfillment of the requirements for the Master of Science degree in Chemistry

© Vincent Saullo 2020

Follow this and additional works at: https://ir.lib.uwo.ca/etd

Part of the Amino Acids, Peptides, and Proteins Commons, and the Analytical Chemistry Commons

Recommended Citation

Saullo, Vincent, "Analysis of Oxidatively Damaged Proteins by Mass Spectrometry" (2020). *Electronic Thesis and Dissertation Repository*. 6823.
https://ir.lib.uwo.ca/etd/6823

This Dissertation/Thesis is brought to you for free and open access by Scholarship@Western. It has been accepted for inclusion in Electronic Thesis and Dissertation Repository by an authorized administrator of Scholarship@Western. For more information, please contact wlswadmin@uwo.ca.

Abstract

As humans age, exposure to oxidative stress may induce protein degradation or aggregation; both resulting in loss of protein function. Protein oxidative damage remains a dominant pathology in many common ailments. To combat these pathologies, scientists must understand the nature of oxidative modifications and their effects on protein structure and dynamics. This work employs a range of mass spectrometry (MS) methods to characterize and analyze the effects of oxidative damage on the model protein myoglobin (Mb). Mb was oxidized using tert-butyl hydroperoxide, and the resulting modifications were characterized by top-down and bottom-up MS workflows. Hydrogen/deuterium exchange MS indicated elevated structural dynamics in oxidatively modified regions. Collision-induced activation showed that oxidized Mb loses heme more readily than its unmodified counterpart. Ion mobility experiments uncovered that collision-induced unfolding produces more compact non-native gas phase structures for the oxidized protein. The methods applied provide an analytical foundation for the comprehensive characterization of oxidative damage that will be applicable to many other proteins.

Keywords

Protein oxidation, Protein Dynamics, Mass Spectrometry, Reactive Oxygen Species, Myoglobin, Hydrogen Deuterium Exchange

Summary for Lay Audience

Oxidative damage is the result of an overabundance of reactive oxygen-containing chemicals in the body. These chemicals arise as the result normal cellular processes but can be exacerbated by external factors like smoking or tanning. Antioxidants in the body combat the effects of these chemicals, but an imbalance can result in damaging reactions occurring inside of the body (*i.e., oxidative damage*). As living things age, deterioration of biological processes can be partially attributed to accumulation of oxidatively modified proteins – the biological building block for cells and tissues. Oxidative damage has been implicated as one of the causes of common ailments including glaucoma and neurodegenerative disorders such as Parkinson's and Alzheimer's disease. Looking into the eyes of someone who suffers glaucoma, the direct result of oxidative protein damage can be seen. The cloudiness in the eye is produced by the accumulation of proteins that have lost function due to extensive oxidation, unrepairable by the body.

This work aims to examine the factors that lead to the disfunction of proteins after oxidative damage. Working with oxidized proteins poses difficulty because they tend to cause problems for many conventional analytical methods; one of these difficulties is their non-uniform mass distribution. Here, we developed a procedure that mimics the effects of reactive oxygen species in the body. Mass spectrometry (MS), a method involving the characterization of gaseous protein ions produced by electrospray ionization, proved to be a versatile approach that allowed us to accurately assess modifications. By applying various MS methods, we were able to determine the chemical nature of modifications, their locations, and their effects on protein structure and dynamics. In this way it was possible to obtain valuable information that might one day help with the development of treatments to combat oxidative damage. Earlier MS studies have produced valuable information on oxidized proteins but neglected certain methods due to onerous data analysis. The current work addresses many of these difficulties, thereby establishing a comprehensive MS-based platform for the characterization of oxidatively damaged proteins.

Acknowledgments

First and foremost, I’d like to express how grateful I am to have studied under Dr. Lars Konermann. Lars’ enthusiasm for science made these two years incredibly valuable and has nurtured my own love for science. It is always important for leaders to express their curiosity and love for what they do as it inspires new generations of scientists. Lars embodies this in everything he does. Lars inspires me to use everything I have learned and spread my love for science and inquisition to those around me.

Over these years, Lars’ lab has produced some fantastic scientists that I am privileged to have been able to work with. An overwhelming thank-you to Victor, Haidy and Yiming who trained and produced a strong foundation for me, always being present and willing to discuss new ideas, leading me discover new ways to think critically. Leanne, Maryam, Angela, Elnaz, Nastaran, Pablo, Drishti, Derek, Alex, Justin and my new friends overseas; Quentin, Insa and Liwen, all played a pivotal role in making this experience unforgettable. Starting at the University of Western Ontario marked my first time moving away from home and the Konermann Lab welcomed me with open arms.

This journey was made possible by continuous love from my family; Connie, Frank, and Luigi, my grandparents who always checked in on me, all the Maple boys back home, and my incredibly supportive girlfriend Julianna. My roommates Patrick (and puppy June) and all the new friends I’ve made in London provided an invaluable experience and helped me maintain composure.

Last but not least, the Brothers of Kappa Sigma. Near and far, this fellowship helped turn me into the man I am today, and I am so thankful for all I have learned from those around me. Kappa Sigma afforded me leadership opportunities I never would have thought possible when I was just a meek chemistry student at York University. Being part of the Kappa Sigma Fraternity and being embraced by Brothers from all over the world inspires me to be diligent and committed to everything I do. ΑΕΚΔΒ.

Table of Contents

Abstract ... i

Summary for Lay Audience ... ii

Acknowledgments ... iii

Table of Contents ... iv

List of Abbreviations, Symbols, Nomenclature ... vii

Chapter 1 - Introduction ... 1

- 1.1 Proteins ... 1
  - 1.1.1 Structure ... 1
  - 1.1.2 Protein Dynamics ... 4
  - 1.1.3 Protein Oxidative Damage ... 5
  - 1.1.4 Myoglobin ... 7
- 1.2 Classical Methods for Protein Structural Analysis ... 8
  - 1.2.1 UV-Vis Spectroscopy ... 8
  - 1.2.2 Circular Dichroism (CD) Spectroscopy ... 9
  - 1.2.3 Nuclear Magnetic Resonance (NMR) Spectroscopy ... 10
  - 1.2.4 X-Ray Crystallography ... 11
- 1.3 Mass Spectrometry ... 11
  - 1.3.1 Electrospray Ionization (ESI) ... 12
  - 1.3.2 Mass Analyzer ... 15
  - 1.3.3 Protein Mass Spectrometry ... 19
- 1.4 H/D Exchange Mass Spectrometry ... 23
  - 1.4.1 Fundamentals ... 23
  - 1.4.2 HDX Mechanisms ... 24
  - 1.4.3 HDX Data Analysis ... 27

1.5 Scope of Thesis 29

1.6 References 30

2 Analysis of Oxidatively Modified Myoglobin by Complementary Mass Spectrometry Techniques 44

2.1 Introduction 44

2.2 Methods 47

2.2.1 Materials 47

2.2.2 Protein Oxidation 47

2.2.3 Isotopic Modelling 48

2.2.4 Tryptic Digestion 48

2.2.5 Covalent Labelling of Oxidatively Modified Protein 48

2.2.6 Top-Down CID-IM-MS 48

2.2.7 HDX/MS 49

2.2.8 Collision Induced Unfolding - IMS 50

2.2.9 Collision Induced Dissociation 50

2.3 Results and Discussion 51

2.3.1 Oxidation of Myoglobin 51

2.3.2 Characterization of Oxidative Modifications by Bottom-Up MS 55

2.3.3 Covalent Labelling of Oxidized Mb with GRT 58

2.3.4 Characterization of Oxidized Mb by Top-Down CID-IM/MS 60

2.3.5 Analysis of Protein Dynamics by HDX-MS 63

2.3.6 Oxidation Effects on the Behavior of Electrosprayed Mb Ions in the Gas Phase 65

2.4 Conclusions 72

2.5 References 74

3 Conclusions and Future Work 78

3.1 Conclusions 78

3.2 Future Work 79

3.3 References 81

4 Curriculum Vitae 82

Education 82

Awards and Acknowledgements 82

Experience 83

Conference Presentations 83

Course Work - UWO 83

List of Abbreviations, Symbols, Nomenclature

A	Absorbance
CCS	Collisional cross section
CD	Circular dichroism
CID	Collision induced dissociation
CIU	Collision induced unfolding
D_t	Percentage of deuteration
DTIMS	Drift tube ion mobility spectroscopy
FTICR	Fourier transform ion cyclotron resonance
GC	Gas chromatography
HDX	Hydrogen deuterium exchange
HPLC	High pressure liquid chromatography
IMS	Ion mobility spectrometry
IR	Infrared
k_{ch}	Chemical rate constant
k_{cl}	Hydrogen bond closing rate constant
k_{HDX}	Overall hydrogen deuterium exchange rate constant
k_{op}	Hydrogen bond opening rate constant
LC	Liquid chromatography
m	Mass

m/z	Mass charge ratio
MS	Mass Spectrometry
nm	Nanometers
NMR	Nuclear magnetic resonance
PDB	Protein data bank
RF	Radio frequency
ROS	Reactive oxygen species
TBHP	*tert*-butyl hydrogen peroxide
UPLC	Ultra performance liquid chromatography
UV-vis	Ultraviolet-visible spectroscopy
z	Charge

Chapter 1 - Introduction

1.1 Proteins

Proteins are among the key building block of all living organisms. Within the cell, proteins are responsible for a variety of roles encompassing signaling, catalysis, host defense, and transport.[1,2] Given their diverse functions, fascination with proteins continuously grows, spanning multiple fields of study that range from basic physical chemistry to clinical research. Protein misfunction is linked to numerous diseases, creating an urgent need to better understand the fundamentals of protein structure and dyamics.[3–11]

1.1.1 Structure

Proteins are assembled by translation of mRNA at a ribosome, resulting in the creation of a polymeric chain of L-amino acids. Amino acids are composed of three main components: an amine group, a carboxylic acid group and a chiral α-carbon bearing a sidechain (*"R" group*). When any two of the 20 possible amino acids bind together, they produce a peptide bond through the formation of an amide between the carboxylic acid group of one amino acid and amine group of the next (Figure 1). These peptide bonds exhibit partial double bond character, forcing the adjacent six atoms into a plane.

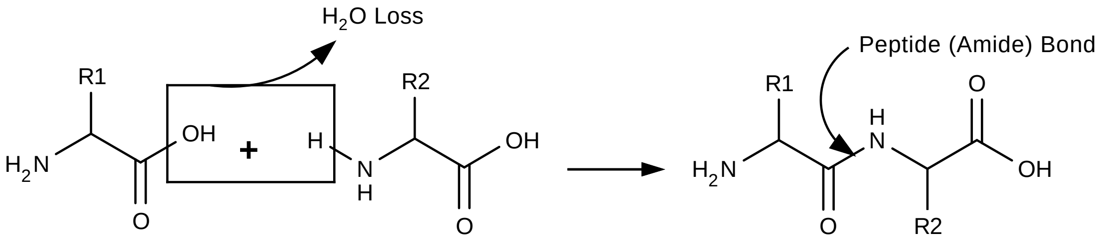

Figure 1: *Amide bond formation between two amino acids.*

The primary structure (amino acid sequence) serves as a unique identifier of each protein; this sequence dictates the protein folding behavior and therefore determines the final protein structure (Figure 2A). The conformational freedom of polypeptide chains arises primarily from rotation of the dihedral angles ϕ and ψ on either side of α-carbons.[12] As the backbone arranges itself during the folding process, numerous intramolecular hydrogen bonds form between backbone NH and CO groups. These hydrogen bonds give rise to two particularly favorable secondary structures; α-helices and β-sheets (Figure 2B).[13,14]

Protein tertiary structures are further stabilized by disulfide bonds, hydrophobic contacts, salt bridges, and van der Waals contacts (Figure 2C).[15,16] Natively folded proteins can also incorporate organic or inorganic moieties to introduce new functionality. Cofactors, such as heme, allow many proteins (e.g., hemoglobin, cytochrome *c* and myoglobin) to perform functions that go beyond features mediated by amino acid side chains. Quaternary structure refers to the oligomerization of two or more polypeptide chains into higher order complexes (Figure 2D). These subunits assemble through intermolecular contacts, forming complexes with diverse functions.[17] Scientists have developed computer programs in an attempt to predict protein tertiary and quaternary structures (as well as protein function) on the basis of amino acid sequences. However, such sequence-based prediction algorithms are still at a relatively early stage of development.[18,19]

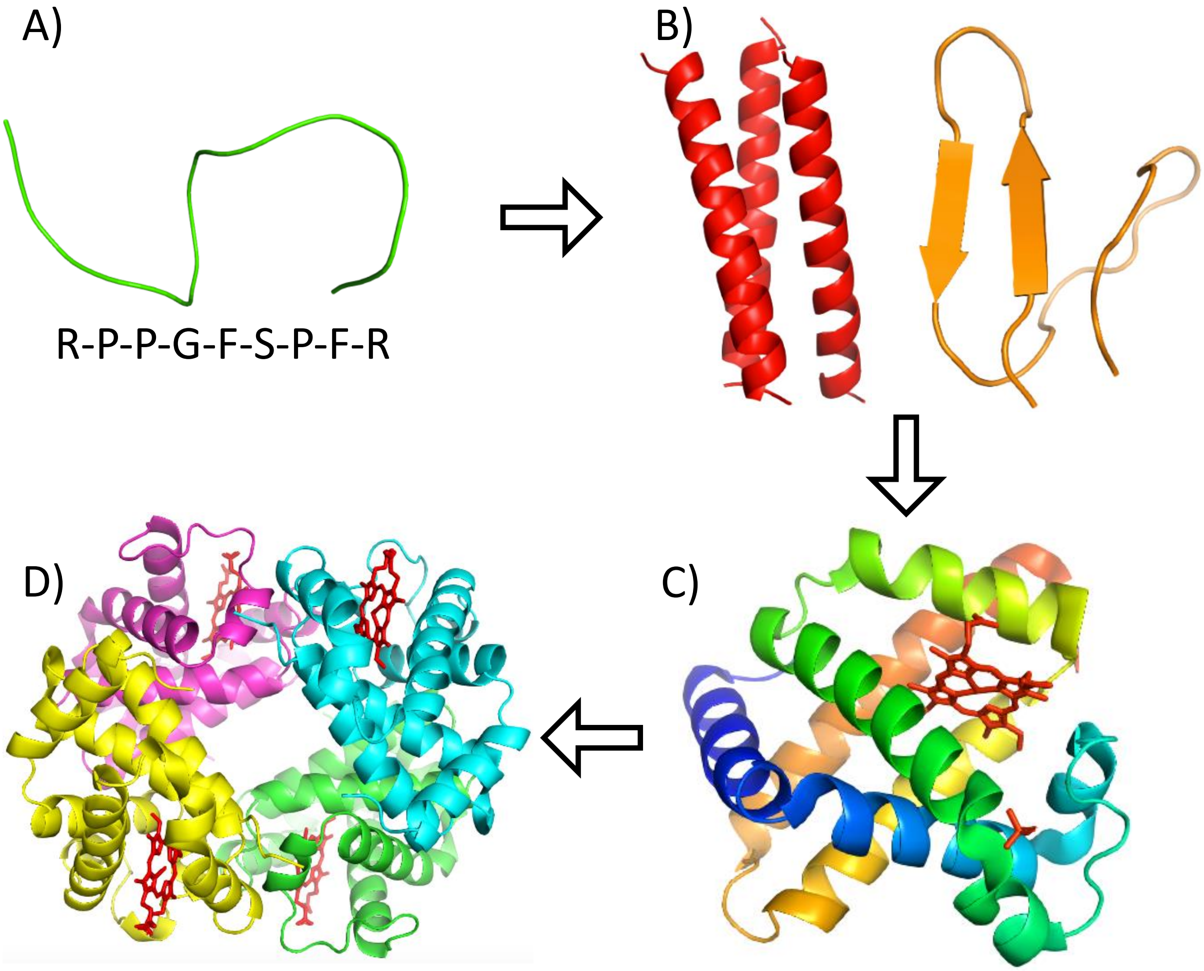

Figure 2: *Different levels of protein structure. A) Primary structure: the sequence of amino acids building a protein (PDB:6F3V). B) Secondary structure: hydrogen bonds create ordered structures in terms of α-helices (red - PDB:1COS) and β-pleated sheets (orange – PDB:1ICL). C) Tertiary structure: intramolecular side chain interactions produce a folded protein (PDB:1WLA). D) Quaternary structure: the assembly of multiple amino acid chains and subunits (indicated by different colour) into a larger structure (PDB:1A3N).*

1.1.2 Protein Dynamics

Seminal studies by scientists such as Kendrew, Ramachandran and Pauling uncovered the fundamentals of protein structure. However, even the availability of high-resolution X-ray structures does not necessarily reveal the biological functions of proteins.[12,14,20] This is because protein function is usually not mediated by static structural features (such as those seen in X-ray crystallography). Instead, the key to understanding protein function lies in protein dynamics, i.e., structural fluctuations that take place on multiple time scales, from picoseconds to seconds.[1,17] Unravelling how protein conformers dynamically interact with the surrounding solvent, substrates, and other proteins is essential for understanding biological systems.

The dynamics of a protein can be visualized as an amalgamation of kinetics and thermodynamics, where the protein continuously moves through its various Boltzmann-allowed conformations on the free energy landscape. Conformations with low free energy values are thermodynamically preferred, but higher energy states are populated as well with certain probabilities that scale as $\exp(-\Delta G/RT)$, where ΔG is the free energy difference relative to the ground state.[21,22] Interactions with ligands can affect the conformational free energy, thereby either stabilizing or destabilizing various forms.

In enzymes, structural motifs fold into specific catalytically active sites. Dynamic conformational motions are essential for enzyme-substrate interactions such that active sites can adopt conformations that are required for catalysis.[23,24] The binding of substrates often produces “induced fit” conformational changes that allow catalytic events to take place.[25,26] Motor proteins exemplify the relationship between dynamics and function particularly well, as they convert one form of energy into another. For example, F_0F_1 ATP Synthase harnesses a proton-motive force to drive the movement of a central rotor, thereby generating ATP.[27–30]

Another example is hemoglobin, where the initial binding of O_2 to a heme-cofactor induces a conformational change, as outlined by the Perutz mechanism.[31–34] Binding of the first O_2 to the heme iron of the completely deoxygenated (*T-state*) protein induces a conformational change in the heme porphyrin plane. This event is transmitted via the distal histidine and propagates through the entire protein, thereby cooperatively enhancing the favorability of O_2 binding at the remaining three subunits. Eventually, these events produce the fully oxygenated *R-state*.[35] The binding of effectors can trigger allosteric effects far away from the effector binding site. For example, effector binding can induce conformational changes that open or close binding regions elsewhere in the protein, providing the foundation of various biological regulation effects such as enzyme activation or deactivation.[31,36–39] Allosteric interactions are also important for various drug action mechanisms.[40,41]

Considering how dependent protein function is on conformational dynamics, any factor that alters the structure and dynamics of the native state will likely be detrimental to normal function. Oxidative modifications are of paramount importance in this context, as outlined in the following section.

1.1.3 Protein Oxidative Damage

Protein oxidative damage represents an intriguing physiological phenomenon. Oxidative stress arises from an imbalance of reactive oxygen species (ROS) relative to antioxidant defense mechanisms within the body. These imbalances lead to biomolecular damage that adversely affects cellular functions.[42–45] ROS include H_2O_2, and ROOH, but also free radicals such as $O_2^{\bullet -}$, $^{\bullet}OH$, and $RO^{\bullet}$. These species can arise from both endogenous and exogenous effects.[46] Endogenously, ROS are generated during processes such as cellular respiration, NADPH oxidase oxidation, and peroxidation.[46–50] Exogenous factors such as smoking and excessive radiation (e.g., tanning, X-rays) also contribute to ROS generation.[46–49] ROS serve important physiological roles. In immune defense, neutrophils and eosinophils utilize myeloperoxidase and eosinophil peroxidase, respectively, to produce ROS for combating pathogens.[47,51] ROS also serve a role during reversible oxidation of cysteine and methionine in cell signaling.[46,52–55]

ROS have been implicated as one of the causes of common ailments including neurodegenerative disorders such as Parkinson’s and Alzheimer’s disease, and glaucomatous neurodegeneration.[3,49,56–59] As organisms age, deterioration of biological processes can be partially attributed to accumulation of oxidatively damaged proteisn.[4,58,60] The body defends itself against ROS by diverting glucose 6-phosphate (G6P) from glycolysis into a side reaction - the pentose monophosphate shunt.[50] Here, NADPH is utilized for the reduction of hydrogen peroxide to water by glutathione (GSH) and catalase in different reactions. GSH and superoxide dismutase (SOD) both scavenge free radicals, while catalase breaks down H_2O_2.[44,53,55,61]

High concentrations of ROS induce oxidation of lipids and nucleic acids; however, proteins are the main subject of oxidative damage due to their high abundance,[62] often leading to biomolecular damage that is detrimental to function.[42–45] In proteins, ROS mainly target amino acid side chains (Figure 3), although the backbone is also somewhat susceptible to modification, in particular by $^{\bullet}OH$.[5,60,63] All these modifications can lead to protein destabilization, aggregation and loss of function.[3,5,49,64]

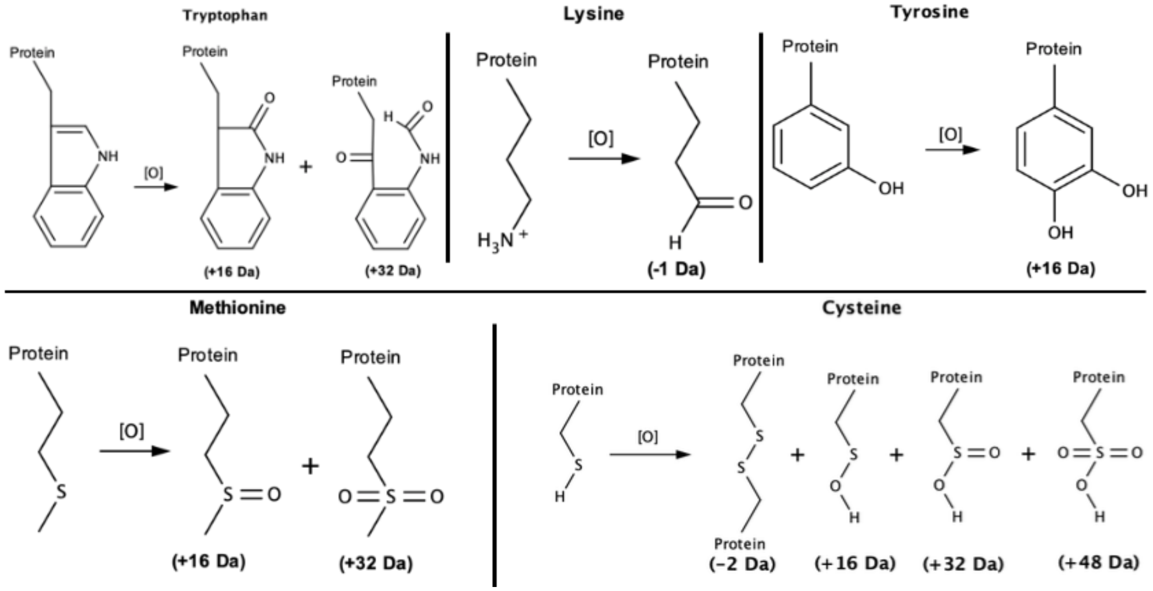
Tryptophan
Protein
NH
[O]
O
+
H
(+16 Da)
(+32 Da)
Lysine
Protein
[O]
H_3N^+
H
O
(-1 Da)
Tyrosine
Protein
[O]
OH
(+16 Da)
Methionine
Protein
[O]
S
S=O
+
O=S=O
(+16 Da)
(+32 Da)
Cysteine
Protein
[O]
S
H
+
(−2 Da)
(+16 Da)
(+32 Da)
(+48 Da)

Figure 3: *Common oxidative side chain oxidations and their associated mass shifts.*

Because of the many deleterious effects of ROS, a large focus has been put on identifying therapeutically effective antioxidants. Resveratrol (3,5,4’-trihydroxy-trans-stilbene), found in the skin of grapes, has promising effects in prolonging life expectancy through modulation of antioxidant metabolism enzymes and scavenging of free radicals.[65–69]

Protein oxidation alters the physicochemical properties of amino acid side chains such as mass, charge, shape, and hydrophobicity. These changes, in turn, affect functional properties including enzymatic activity and drug binding.[1-6,70,62] If an intermediate or unfolded species becomes oxidized, it may lose its ability to refold to the native state due to altered intramolecular interactions. As well, natively folded proteins may unfold as a result of oxidative modifications. Both of these scenarios would most likely result in loss of function.[71–73] If the protein is not subjected to proteasomal degradation and subsequently replaced, successive oxidation events will lead to the accumulation and/or aggregation of non-functional protein (Figure 4). For proteins that are not regenerated in the body (i.e., crystallin in the eye lens), the effects of ROS are accentuated. Crystallins become resistant to proteasomal degradation as a result of aging-related oxidative modification and will accumulate in the eye (cataract formation).[71,74,75] Without the ability to repair or regenerate these proteins, oxidation causes permanent loss of function.[74,76]

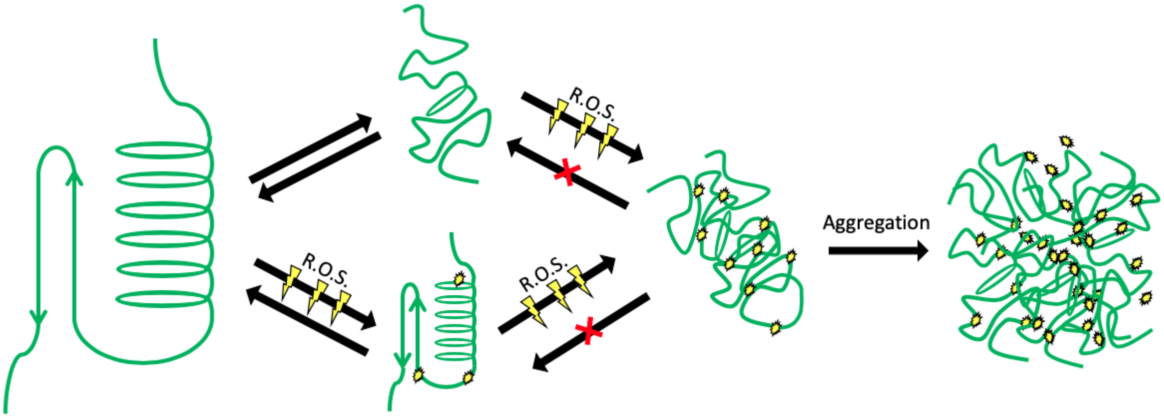

Figure 4: *Both native and unfolded proteins may be subjected to oxidative damage when exposed to ROS. Upon slight oxidation, the protein may maintain its structure but will most likely be subjected to proteolysis. If oxidation products accumulate, the protein may lose the ability to exist in a folding equilibrium. The highly oxidized protein loses function and may become immune to proteolysis, aggregating inside the cell.*

1.1.4 Myoglobin

Myoglobin represents a commonly used model system for experimental studies on protein structure and dynamics.[21,77–85] It has a mass of 17.5 kDa and is composed of 8 α-helices (Figure 5).[86] In its native state, myoglobin exists as heme-bound holo-myoglobin (hMb) – granting it function as an oxygen reservoir in muscle tissue. The heme cofactor is contained within a hydrophobic pocket where it forms multiple noncovalent linkages, along with a coordination bond of the iron center to the proximal His93.[82] Due to the weak nature of the heme-protein interactions, myoglobin may also exist in its heme-free apo form (aMb). Heme loss causes the F helix to partially unfold while leaving the remaining structure relatively similar to native hMb.[77,78,87] In physiologically active hMb the heme is in the Fe^{2+} state, but after prolonged oxygen exposure, iron will oxidize to Fe^{3+}. The formation of metmyoglobin (Fe^{3+} hMb) is responsible for the brownish-red colour seen in aging red meat and is unable to bind O_2.[88,89,90] Increased myoglobin concentration in urine serves as an indicator of muscle injury and renal failure, while the presence of protein-oxidized myoglobin in myocardial tissue has been identified to be indicative of acute myocardial infarction.[91–93]

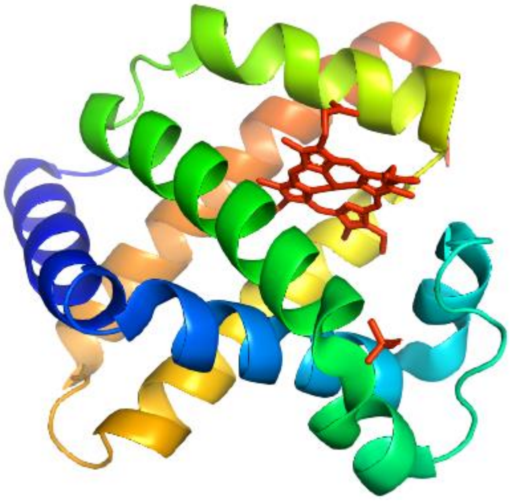

Figure 5: *X-ray crystal structure of myoglobin from horse heart (PDB 1WLA).*

1.2 Classical Methods for Protein Structural Analysis

1.2.1 UV-Vis Spectroscopy

Ultraviolet visible (UV-Vis) absorption spectroscopy uses electromagnetic radiation with wavelengths in the range of 200 to 700 nm. This method is widely employed for quantitative assays involving organic, inorganic and biological analytes.[94]

The Beer-Lambert law (Equation 1.1) establishes the relationship between absorbance (A) and concentration (c) of a chromophore for a certain path length (l). The molar absorption coefficient ε is specific to the sample being measured. In Equation 1.1, I_0 denotes the incident light intensity, while I is the intensity of transmitted light.[95]

$$A = log\frac{I_0}{I} = \varepsilon lc$$

Equation 1.1

UV-Vis spectroscopy is useful for determining protein concentrations by measuring the absorbance at 280 nm, where the aromatic residues tryptophan, phenylalanine and tyrosine absorb, or around 407 nm (Soret region) which is the peak absorbance of heme and related porphyrins.[96,97] UV-Vis spectroscopy provides little direct information about protein structure, however, absorbance changes of cofactors such as heme can report on conformational changes.

1.2.2 Circular Dichroism (CD) Spectroscopy

CD spectroscopy exploits the differential absorption of left and right-circularly polarized light by chiral chromophores.[98,99] This difference (molar ellipticity) is what constitutes a CD spectrum. CD spectroscopy is a valuable tool for the analysis of secondary structure. The absorbance in the far-UV range (180-250 nm) arises from peptide bonds and has characteristic CD signatures depending on the type of secondary structure (Figure 6).[100–102] In addition, CD in the near-UV range (260-320 nm) caused by absorption by aromatic amino acids and S-S bonds, is related to their respective environments and reveals tertiary structural information.[98] CD signals can also be associated with cofactors such as heme in myoglobin or cytochrome *c*. Although specific secondary structures are not always accurately quantifiable, changes in CD spectra are a reliable probe of protein folding or unfolding.

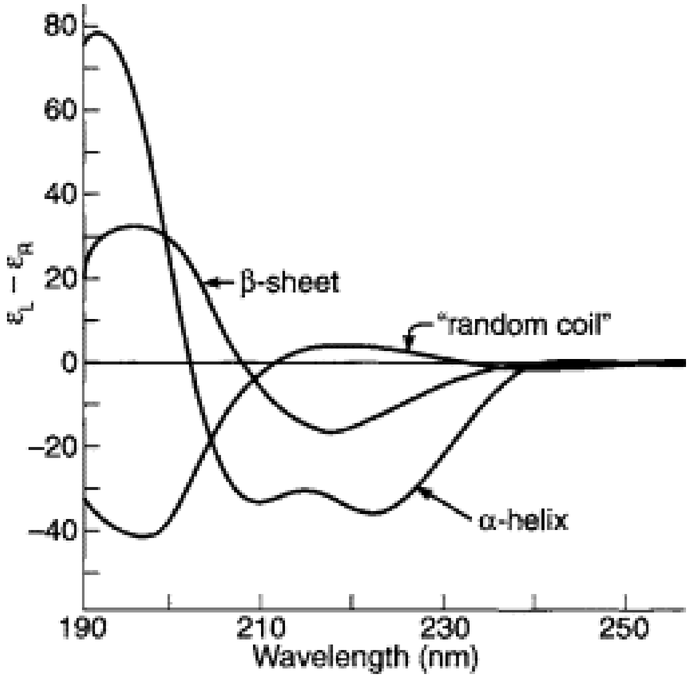

Figure 6: *Different secondary structures produce specific CD spectra.*[103,104] *This figure is reproduced from reference 103.*[103]

1.2.3 Nuclear Magnetic Resonance (NMR) Spectroscopy

Nuclear magnetic resonance (NMR) spectroscopy is one of the most widely used techniques for the structural characterization of small chemical compounds. NMR techniques are based on the absorption of radio-frequency (RF) electromagnetic waves by atomic nuclei – differing from UV-vis and infrared (IR) spectroscopy which focus on the outer electrons.[94] An externally applied magnetic field aligns spin 1/2 nuclei, with the magnetic moments being parallel or antiparallel to the field. Once aligned, the absorption of specific RF frequencies can induce spin flips. The corresponding resonance frequencies depend on the chemical environment of each nucleus, as governed by the presence of other nuclei and the surrounding electrons.[94,105]

Technological advances have drastically improved the ability of NMR spectroscopy to elucidate the 3D structures of proteins. 2D and 3D NOESY (nuclear Overhauser effect spectroscopy) techniques - among other methods - and analyzing different nuclei in addition to ^{1}H, such as ^{13}C and ^{15}N, has proven incredibly useful for protein structural studies. Roughly 10% of the coordinates in the Protein Data Bank (PDB) are NMR structures.[106–108] NMR is also useful for protein dynamic assays since it can use spin relaxation measurements for probing conformational fluctuations.[108] Currently existing limitations of protein NMR spectroscopy include its relatively low sensitivity, implying the need for high analyte concentrations (typically in the high μM to low mM range). Some proteins tend to aggregate under these high concentration conditions. In addition, the applicability of NMR spectroscopy is typically limited to proteins smaller than ~40 kDa.

1.2.4 X-Ray Crystallography

X-ray diffraction is used for the structure determination of crystallized proteins. Inverse Fourier analysis of the measured diffraction pattern yields electron densities that can provide atomically resolved data. For example, John Kendrew solved the structure of sperm whale myoglobin using X-ray crystallography and was co-awarded the 1962 Chemistry Nobel Prize for this achievement.[20] Most of the protein structures in the PDB were generated using X-ray crystallography. In contrast to NMR spectroscopy, X-ray methods can be applied to very large proteins, although, crystallization can be challenging (e.g. for membrane proteins).[109]

1.3 Mass Spectrometry

Mass spectrometry (MS) characterizes gaseous ions on the basis of their mass to charge ratios (*m/z*). MS is revered for its high sensitivity, requiring only small amounts of analyte at low (μM or nM) concentrations. MS can also be paired with complementary analyte separation and analysis techniques such as UV-Vis absorption, gas chromatography (GC) and liquid chromatography (LC). Fragmentation cells or ion mobility analyzers can be added into the mass spectrometer for additional dimensions of analysis.

As MS has matured in recent years, instruments are now available that have a spectral resolution of over a million (resolution is defined by the peak *m/z* divided by the width at 50% height). High resolving power affords the ability to distinguish two peaks of similar *m/z* from each other, unlocking analysis potential beyond that of just large protein complexes.[110]

Mass spectrometers consist of three main components: ion source, mass analyzer and detector. One caveat with MS is that analytes must be transformed into gaseous ions. Up until the 1990s, both of these aspects were problematic for MS analyses of large biological molecules. Ions generated in the source pass into mass analyzers where they are separated based on *m/z*. The ions then reach a detector where they are translated into spectral signals (ion intensity vs *m/z*). These components are discussed in detail in the following sections.

1.3.1 Electrospray Ionization (ESI)

Multiple ionization techniques have been developed that can be applied to different types of samples. These include electron impact (EI), atmospheric pressure chemical ionization (APCI), chemical ionization (CI), and matrix-assisted laser desorption/ionization (MALDI). The most widely used method, however, is electrospray ionization (ESI).

Developed by John Fenn,[111] ESI in combination with MS has cemented itself as one of the most effective methods for protein analysis and earned Fenn the Chemistry Nobel Prize in 2002 (jointly with Koichi Tanaka). Briefly, ESI is an ionization technique that involves the charging of a solution-phase analytes after passing the sample through a charged capillary. In positive-ion-mode the resulting gas phase analyte ions are normally multiply protonated with a mass-charge ratio

$$\frac{m}{z} = \frac{M + z(1.008)}{z}$$

Equation 1.2

where M is the neutral analyte mass, z is the number of charges (charge state) and 1.008 represents the proton mass (Da). Greatly improved analytical workflows can be implemented by coupling high pressure liquid chromatography (HPLC) with ESI-MS for two-dimensional (solution/gas phase) separations.[112] An ESI source in positive ion mode (Figure 7) resembles an electrochemical cell where the metal capillary represents the anode and the mass spectrometer inlet is the cathode. Solution is injected either directly or by HPLC. Charged solution builds up at the tip of the capillary, forming a Taylor Cone. A mist of charged droplet is emitted from the Taylor cone. These droplets undergo solvent evaporation until Coulombic repulsion reaches the surface tension of the solution (a situation known as "Rayleigh Limit", defined by Equation 1.3)[113]

$$z_R = \frac{8\pi}{e}\sqrt{\varepsilon_0 \gamma r^3}$$

Equation 1.3

where z_R is the droplet charge at the Rayleigh limit, e is 1.60×10^{-19} C, ε_0 is the vacuum permittivity constant, γ is the surface tension coefficient, and r is the droplet radius. Droplets at the Rayleigh limit undergo jet fission. Ultimately, the combination of solvent evaporation and fission events generates nanometer-sized droplets from which analyte ions are released into the gas phase.

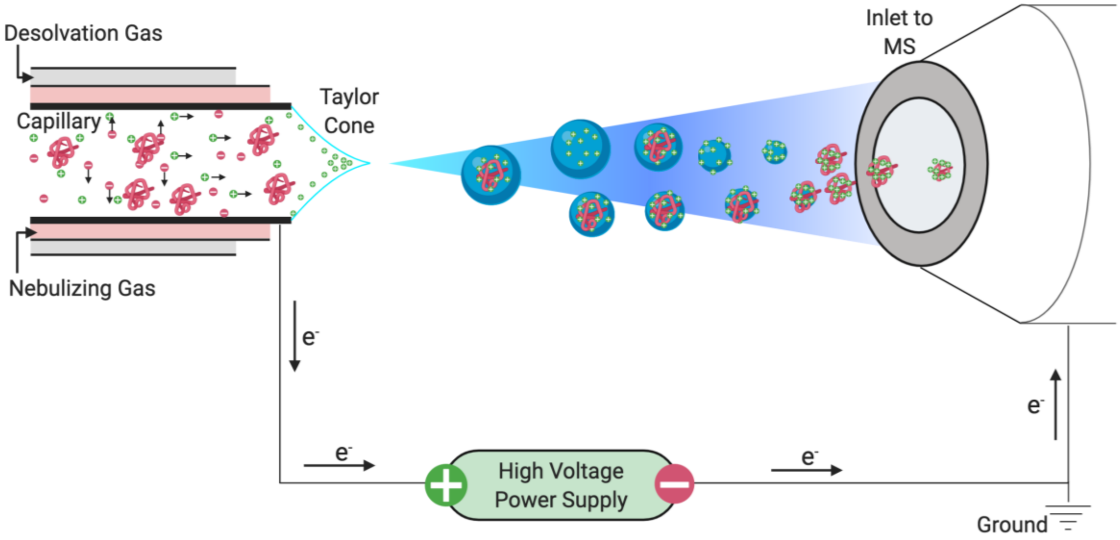

Figure 7: *Schematic depiction of an ESI-source. Analyte solution composed of proteins (red) and ions enter the source via a charged metal capillary and aerosolize before reaching the inlet. Droplets decrease in size as solution evaporates.*

ESI overcomes the difficulties of working with high-mass proteins as they will become highly charged, allowing their detection even on mass spectrometers that have limited *m/z* range.[114] Ion release from highly charged nanodroplets has long been thought to proceed via one of two mechanisms; the Charged Residue Model (CRM)[115] and the Ion Ejection Model (IEM).[116] Recently, Konermann *et al*. have proposed an additional pathway, the Chain Ejection Model (CEM)[117] (Figure 8). The CRM applies mostly to globular protein molecules and states that ESI nanodroplets will dry completely, leaving residual charges on the globular protein.[115] The IEM applies to pre-charged small analytes and ions, proposing that as droplet size shrinks, the repulsive forces cause ions to eject from the droplet surface.[116] The CEM concerns unfolded proteins and large polymers; it is thought that hydrophobic surfaces of the analyte will cause the protein chain to migrate toward the droplet surface. Subsequently, partial ejection of the protein takes place, and charges equilibrate between the droplet and its protruding tail. The protein then separates from the droplet in a charge state that is higher than in its folded counterparts.[117–119]

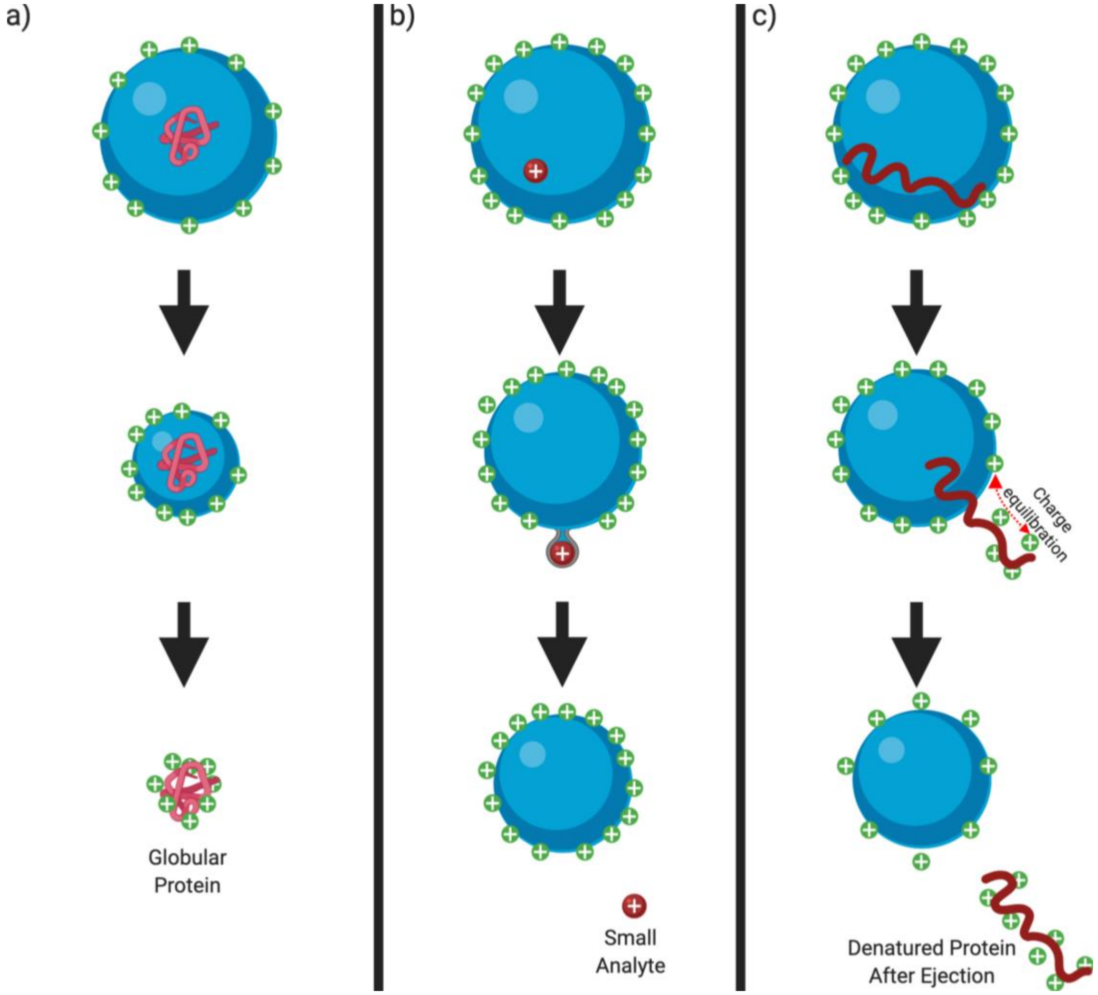
a)
b)
c)
Globular Protein
Small Analyte
Charge equilibration
Denatured Protein After Ejection

Figure 8: Overview of ESI mechanisms. *a) CRM, b) IEM,* ***c)*** *CEM. For details, see text.*

1.3.2 Mass Analyzer

The mass analyzer component separates ions based on their *m/z*. Different mass analyzers are available; they serve different purposes and have different performance characteristics in terms of resolution, transmission efficiency, etc. Common mass analyzers include quadrupoles, time-of-flight (TOF) analyzers, Fourier transform ion cyclotron resonance (FTICR) instruments, and Orbitraps. Only quadrupoles and TOF systems will be briefly discussed.

Mass analyzers can be used to record mass spectra (known as MS^1). Alternatively the mass analyzer can be used for selecting precursor ions with specific *m/z* which are then fragmented, followed by fragment ion analysis on a second mass analyzer (MS/MS or

MS^2), the most common fragmentation method is collision-induced dissociation (CID), which involves the activation of analyte ions via collisions with inert gas atoms. These collisions cause ion heating, allowing them to overcome activation barriers such that decomposition can take place. MS/MS data generated in this way provide information on the structure and chemical composition of analytes, such as the sequence of peptides and proteins.

1.3.2.1 Quadrupoles

Quadrupoles serve important purposes as ion guides, collision cells and as mass filters for precursor ion selection. Quadrupoles have a limited mass range and resolution, but they are well suited for low-mass ions. Quadrupoles consist of four cylindrical rods with applied electrical potentials, AC (or “radio frequency”, RF) and DC voltage, that allow for selective transmission of ions. RF/DC ratios remain constant while the amplitude can be varied to select different *m/z* ranges. For any given RF/DC ratio, only ions of one specific *m/z* adopt a stable trajectory and get transmitted, while other ions become unstable collide with the rods. Quadrupoles can also be operated as RF-only, where almost all *m/z* are transmitted. In this state, the quadrupole can be used as an ion guide or as a collision cell for ion fragmentation.

Quadrupoles are widely used for precursor ion selection in MS/MS experiments, i.e., prior to fragmentation in a collision cell. In triple-quadrupole instruments, the second quadrupole is operated in RF- only mode and serves as collision cell. Quadrupoles can also produce a mass-spectrum by scanning through different voltages in small steps and measuring ion output count with a channel electron multiplier. In summary, quadrupoles are highly versatile, making them a common component of various types of mass spectrometers.

1.3.2.2 Time of Flight Mass Spectrometry (TOF-MS)

TOF mass spectrometers have a flight tube of length l, in which ions are propelled through a field-free vacuum with a velocity (v) that depends on *m/z* (Equation 1.4). An electrostatic pusher applies a uniform orthogonal acceleration voltage pulse ΔU. Subsequently, the potential energy of the ion ($\Delta U\, z\, e$) is converted to kinetic energy ($1/2mv^2$) such that

$$\frac{l}{t_{flight}} = v = \sqrt{\frac{2\Delta Uze}{m}}$$

Equation 1.4

Simple linear TOF analyzers have high transmission but low resolution (~2000). Much higher resolution (20000 and higher) can be obtained on a reflectron-TOF system (Figure 9). Reflectrons act as electrostatic mirrors that reverse the flight direction of ions, based on electric potentials applied to the stack of rings that constitutes the reflectron. Reflectrons address the problem that ions of the same *m/z* can be accelerated to slightly different kinetic energies in the pusher, thereby causing peak broadening due to different arrival times. The reflectron corrects for these differences as ions with the same *m/z* but different kinetic energy will penetrate the reflectron to different depths, thereby ensuring that the ions reach the detector after the same time of flight.

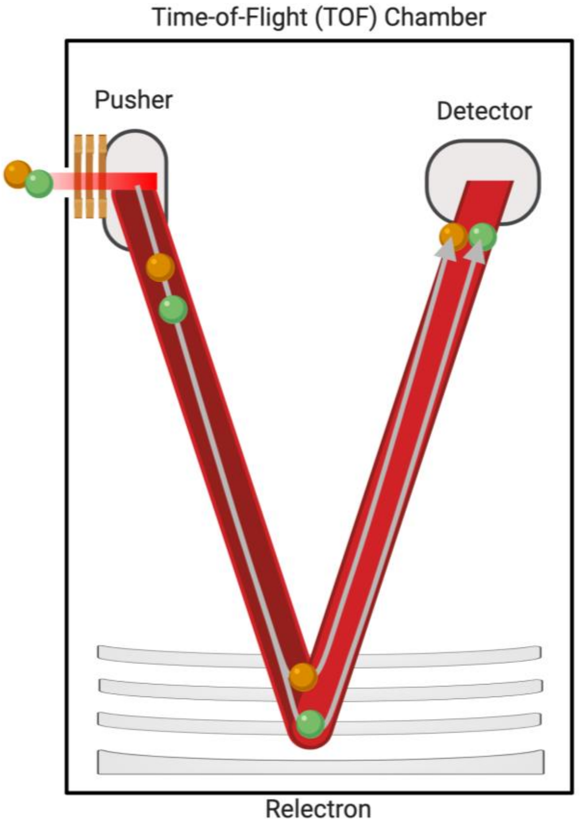

Figure 9: *Schematic cartoon of a reflectron-TOF. Ions enter the TOF chamber and are accelerated with a potential energy,* ΔU**,** *applied by the pusher. Ions penetrate the reflectron to different depths, based on their velocities.*

By combining these components, ESI-Q-TOF mass spectrometers (Figure 10) are commonly used by industry professionals and academics alike. From left to right, an analyte is ionized via an ESI source and sprayed towards the inlet cone. Ions then selectively pass through a quadrupole mass analyzer and into the trap where ions may be fragmented and further separated through an (optional) ion mobility chamber. Passing through the transfer cell, the ions are given a pulse of energy through the pusher and enter the TOF flight tube where they are further separated before reaching the detector. For MS/MS analyses, the quadrupole is used to select specific precursor ions (MS^1) for fragmentation in the trap or transfer cell. The fragments will then be analyzed by the TOF (MS^2) to complete tandem mass spectrometry. The time it takes for an ion to travel from the pusher to the detector depends on *m/z* and is described by rearrangement of Equation 1.4 into Equation 1.5:

$$\sqrt{\frac{m}{z}} = \frac{t_{flight}\sqrt{2eU}}{l}$$

Equation 1.5

Ions of the same *m/z* are tallied by the detector to create a mass spectrum with *m/z* on the x-axis and counts per second (ion intensity) on the y-axis.

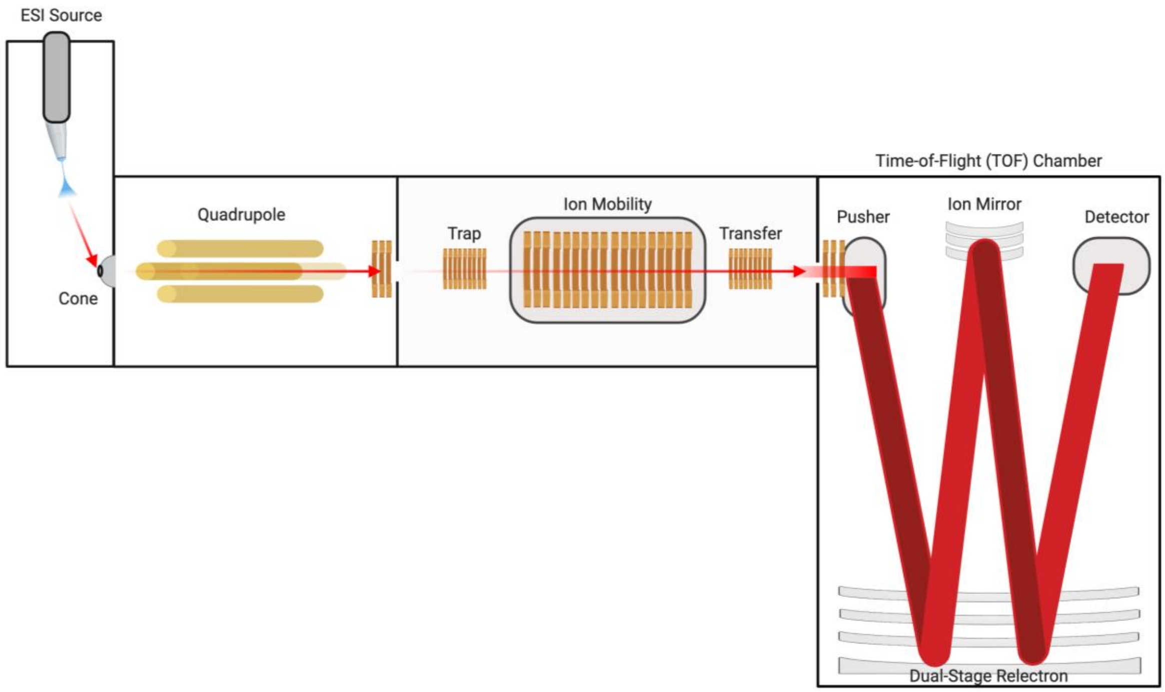
ESI Source
Cone
Quadrupole
Trap
Ion Mobility
Transfer
Time-of-Flight (TOF) Chamber
Pusher
Ion Mirror
Detector
Dual-Stage Relectron

Figure 10: *Schematic diagram of a quadrupole-time-of-flight (Q-TOF) mass spectrometer.*

1.3.3 Protein Mass Spectrometry

MS has become widely adopted in proteomics and biophysical chemistry due to its robustness, sensitivity, accuracy, and the versatility offered by different MS workflows.

Passing the samples through an LC column prior to ESI desalts and purifies analytes, thereby generating spectra that have high S/N ratios (Figure 11).

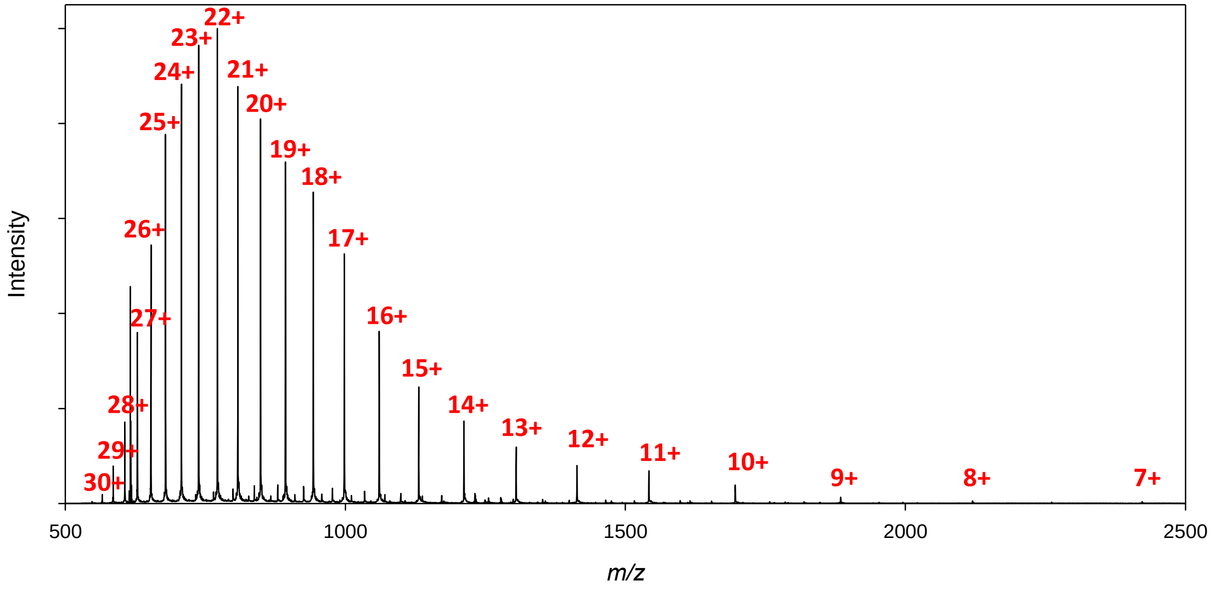

Figure 11: *ESI mass spectrum of acid-denatured aMb acquired on a Waters Synapt G2 following HPLC separation. Charge states z of the individual ions are indicated in red.*

In addition to providing a mass readout, MS instrumentation has developed to be able to analyze structure and dynamics, quantify, visualize and identify increasingly complex samples.[110] ESI-MS also has the ability to analyze proteins in their native conformations using gentle conditions that preserve biomolecular structures and interactions.

One focus area of this thesis is the identification of protein covalent modifications and assessment of the subsequent effects on protein structure and dynamics. Below, two of the most common MS methods for identifying such covalent modification are briefly discussed.

1.3.3.1 Bottom-Up vs. Top-Down Workflows

Two main forms of MS/MS can be distinguished, referred to as bottom-up and top-down MS. Bottom-up MS employs a protease to digest the protein of interest into peptides prior to separation on an LC column, with subsequent ESI-MS/MS analysis (Figure 12). Trypsin is especially useful for determining protein modifications and structure since it is a selective protease that only cleaves after lysine and arginine.[120,121] However, cleavage efficiencies can be perturbed by covalent modification of the positively-charged Lys or Arg side chains.[122,123] Bottom-up MS has become standard practice in most MS workflows because of the dense, site-specific resolution it can provide when coupled to chemical labelling methods.[124,125] In less well-behaved systems, different proteases may be used in combination to increase digestion efficiency and sequence coverage.

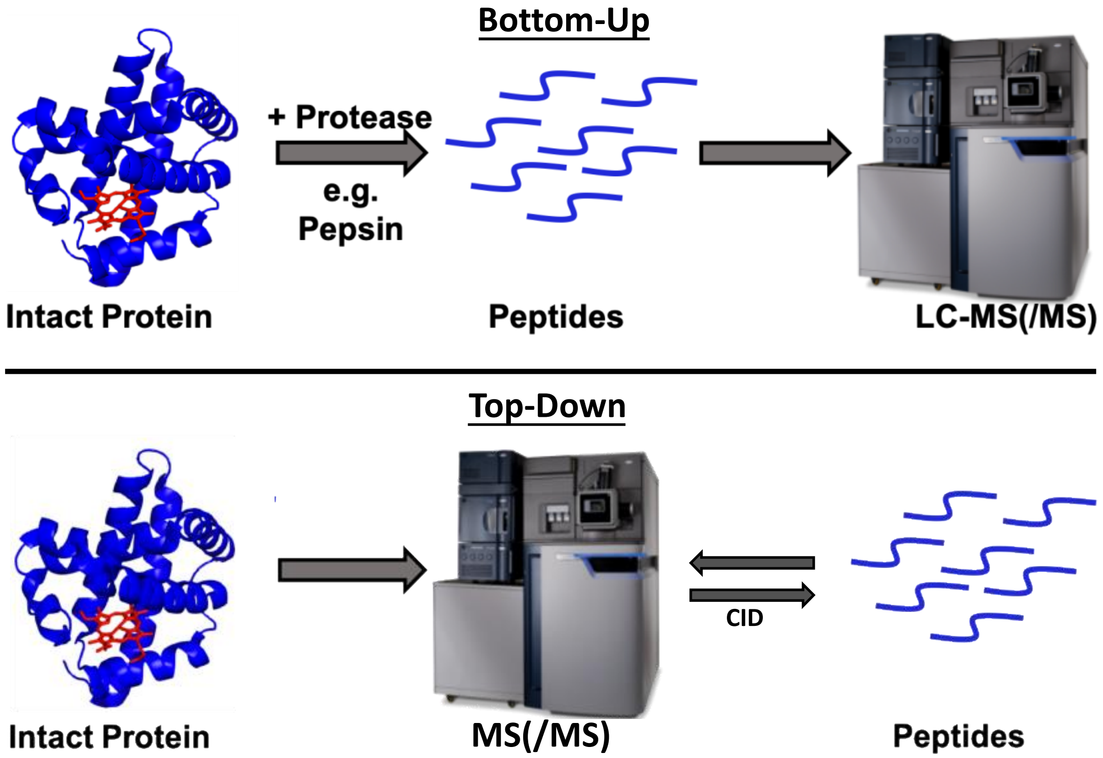

Figure 12: *Both bottom-up and top-down mass spectrometry workflows. In bottom-up, the protein is digested by a protease (e.g., pepsin or trypsin) to create peptides prior to separation on an LC column that is coupled to the mass spectrometer. In top-down, the intact protein enters the mass spectrometer without prior digestion. Instead, the protein is fragmented in the gas phase.*

Rather than employing enzymatic proteolysis, top-down MS involves the fragmentation of intact protein via application of techniques such as CID, ETD (electron-transfer dissociation) or ECD (electron-capture dissociation). In other words, peptides are generated in the gas phase rather than in solution.[126–128] Pairing top-down MS with ion mobility spectrometry (IMS) delivers better resolved peptides, increasing quality of data.

1.3.3.2 Ion-Mobility Mass Spectrometry

Ion-mobility spectrometry (IMS) is a gas-phase separation technique that analyzes ions based on their collisional-cross-section (CCS) and their charge. CCS characterizes the cross-sectional area (i.e., shadow or profile) of an analyte as it passes through the drift tube interacting with inert gas. IMS offers a complementary dimension of analysis that can differentiate between isomers and conformers, normally unapproachable with traditional MS methods.[129–131] Combining IMS with LC/MS(MS) provides multidimensional assays that offer the ability to decipher very complicated analyte mixtures. IMS is commonly used in the context of screening for illicit drugs and explosives.

IMS involves a drift tube with a homogenous electric field in the presence of a background buffer gas (Figure 13). The electric field causes the ions to drift, resulting in separation based on different drift velocities. Cyclic-IMS devices have recently been developed to achieve unprecedented IMS resolution.[132,133]

Different types of IMS instruments have been implemented. For example, drift-tube IMS employs a drift tube with a constant field where analytes are in constant axial motion and separated based on CCS and drift time.[134,135] In contrast, travelling wave IMS (TWIMS) employs an alternating electrical field (Figure 13). Ions enter the travelling wave ion guide (TWIG) where axial motion is opposed by a drift gas (e.g., N_2). RF voltages on the electrodes prevent ions from moving in a radial direction, while pulsed DC current moves ions axially through the opposing drift gas. Because ions only move when acted upon by the electrical field, TWIMS allows for shorter drift tubes while still achieving separation.[136–139]

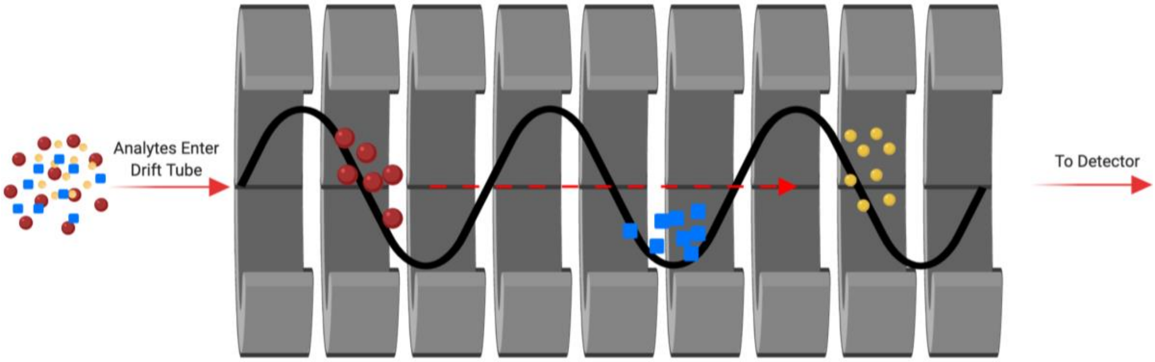

Figure 13: *Schematic diagram of a travelling wave ion mobility device (TWIMS). Analytes enter a gas-filled ion guide drift tube and are separated by a pulsating electric field as they travel toward the detector.*

1.4 H/D Exchange Mass Spectrometry

1.4.1 Fundamentals

H/D exchange (HDX) methods are widely used for studying protein structure and dynamics. Deuterium, ^{2}H, is a heavy isotope of hydrogen that can exchange with hydrogen atoms in NH/OH/SH bonds.[139] This isotopic labelling opens the possibility to an array of different experiments whereby the difference caused by deuteration can be assessed using various tools such as NMR or infrared spectroscopy. Most commonly, HDX experiments are performed with MS detection, and HDX-MS has become a rapidly growing analysis technique for studying protein folding, dynamics, and interactions.[140]

Linderstrøm-Lang pioneered the use of HDX for protein analyses in the mid 20th century when working with insulin.[141,142] The possibility of being able to study the single-residue exchange kinetics by NMR methods was a breakthrough in the 1970s.[143,144] Further breakthroughs came several years later with the advent of multidimensional NMR methods.[145] Today, HDX is dominated by LC-MS-based workflows. LC-MS offers the ability for peptide level resolution when paired with an acidic protease such as pepsin, thereby creating spatially resolved data that reflect dynamic properties of proteins.

1.4.2 HDX Mechanisms

When a protein is fully unfolded and solvent exposed, the N-H → N-D amide hydrogen transitions take place with a rate constant k_{ch}, referred to as the "chemical" rate constant. Conversely, the N-H → N-D transition in highly ordered regions is tempered by protein conformation and hydrogen bonds involving the amide hydrogen. These protective factors cause the deuterium exchange rate constant to fall below that of k_{ch}, resulting in an overall rate constant k_{HDX} (with $k_{HDX} << k_{ch}$). As proteins fluctuate between different allowed conformations, various short-lived '*open'* states exist that allow HDX to take place, before returning to a *'closed'* conformation. These opening and closing transitions have rate constants k_{op} and k_{cl}, respectively. Therefore, the overall deuterium exchange mechanism can be described as

$$N-H_{Closed} \underset{k_{cl}}{\overset{k_{op}}{\rightleftarrows}} N-H_{open} \underset{D_2O}{\overset{k_{ch}}{\longrightarrow}} N-D_{open} \underset{k_{op}}{\overset{k_{cl}}{\rightleftarrows}} N-D_{closed}$$ [146]

Equation 1.6

where the HDX rate constant is

$$k_{HDX} = \frac{k_{ch}k_{op}}{k_{ch}+k_{cl}+k_{op}}$$

Equation 1.7

HDX can take place in two different kinetic regimes, EX1 and EX2.[147,148] Simply put, EX1 gives rise to bimodal mass distribution due to complete deuteration of open states prior to protein refolding ($k_{ch} >> k_{cl}$) such that Equation 1.7 simplifies to

$$k_{HDX} = k_{op}$$

Equation 1.8

In contrast, EX2 shows mass distributions with progressive shifts because deuteration takes place slower than closing ($k_{cl} >> k_{ch}$). Under these conditions HDX proceeds with a rate constant

$$k_{HDX} = K_{op} k_{ch}$$

Equation 1.9

where K_{op} = (k_{op}/k_{cl}) represents the equilibrium constant of bond opening. Figure14 provides a visual representation of these two exchange regimes.

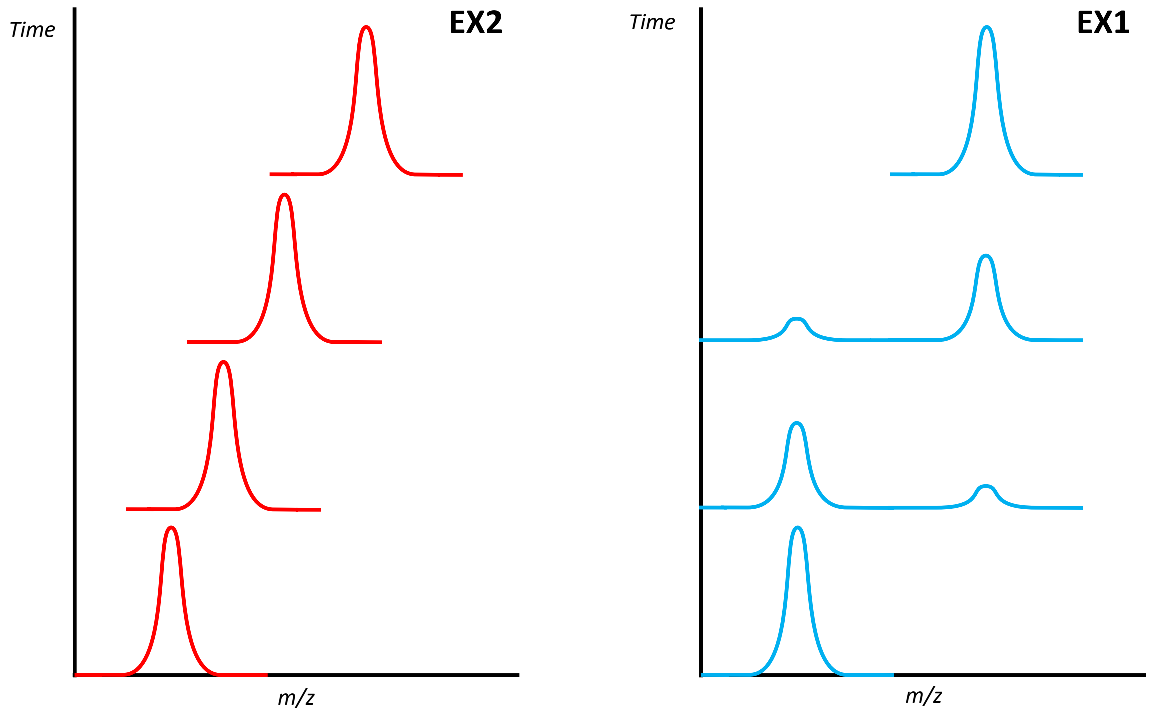

Figure 14: *The EX2 regime (left) describes continuous HDX under conditions where* $k_{cl} >> k_{ch}$*. The EX1 mechanism (right) applies if* $k_{cl} << k_{ch}$ *giving rise to bimodal deuterium uptake distributions.*

HDX is initiated when proteins are exposed to a D_2O-based labelling buffer. This step can happen by exposing the sample to a perturbing agent for a brief amount of time before pulsing with D_2O and quenching (pulse labelling). Alternatively, a protein can be continuously incubated in labelling buffer, while aliquots are taken at specific time points (continuous labelling).[151] Depending on the type of information desired, local (peptide/residue level) or global (intact protein) analysis can be conducted by using either MALDI-MS or LC-MS.

Interaction with HDX buffer causes exchange of labile hydrogens in the amide backbone and in side chains.[141] Side chain deuterium is lost during reverse-phase LC, but backbone amide deuterium can be mostly retained and analyzed by ESI-MS.[152–154] HDX rates depend on pH and temperature, as well as flanking side chains.[146,153–155] This implies that it is imperative to control experimental factors such as pH, quenching temperature, LC and column temperature.[156] Exchange is slowest at pH ~2.5 where k_{ch} attains its minimum (Figure 15) between acid, base and water catalysis (Equation 1.10) thus presenting an optimum range for quenching and analysis.[96, 97]

$$k_{ch} = k_{acid}[H^+] + k_{base}[OH^-] + k_w[H_2O]$$

Equation 1.10

The dependence on temperature can be approximated by the Arrhenius equation

$$k_{ch} = Ae^{-\frac{E_a}{RT}}$$

Equation 1.11

where A is a constant pre-exponential factor, E_a is activation energy, R is the gas constant and T is the temperature.[158] Hence, HDX quenching is performed by lowering the solution temperature to ~0° C, in conjunction with acidification. The quenched samples can then be stored in liquid nitrogen prior to analysis.

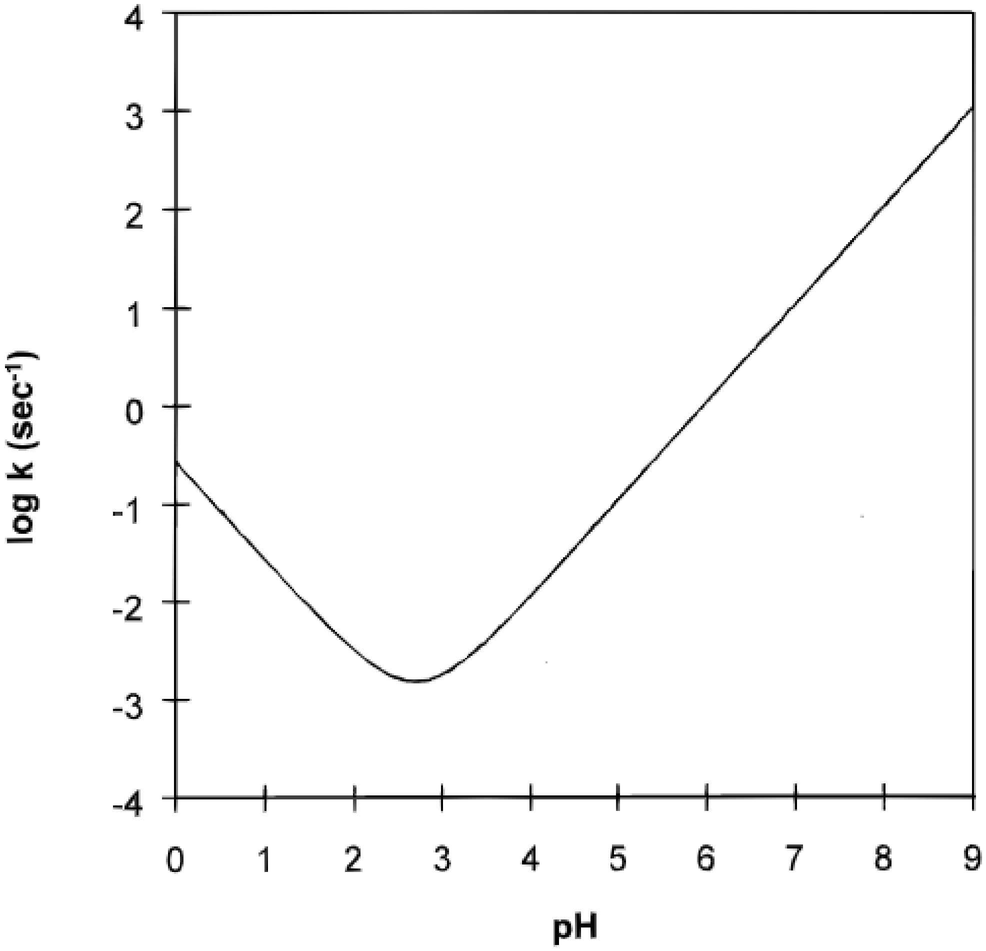

Figure 15: *Dependence of k_{ch} on pH, revealing the existence of a global minimum at around pH 2.4-3. This presents the pH used for HDX quenching.*[157] *This figure is reproduced from reference.*[157]

1.4.3 HDX Data Analysis

HDX-MS is usually performed in a bottom-up fashion.[159] In these experiments, a protease (usually pepsin) is used to create peptide fragments from a protein after HDX, resulting spatially-resolved data. Top-down HDX-MS represents an alternative workflow that uses gas phase fragmentation of proteins without prior proteolysis, but this approach is less commonly applied.[160] In this thesis we will focus exclusively on continuous bottom-up HDX-MS.

Although efforts are made to minimize back exchange during LC, some level of deuterium loss is unavoidable. To account for these effects, two control measurements are performed in addition to the "regular" HDX time points. m_{100} represents a fully deuterated sample, and m_0, which represents an ambient baseline of deuteration under quenched conditions. The equation for percentage of deuteration (D_t) for any time point (t) is then calculated as

$$D_t = \frac{m_t - m_0}{m_{100} - m_0} \times 100\%$$

Equation 1.12

where *m* represents the observed centroid mass of the peptide.[161,162] Generally, D_t will be presented as a function of exposure time for individual peptides. Creating and comparing uptake plots and superimposing the results on protein PDB structures using a colour gradient can help visualize uptake differences. The effects of oxidative damage can then be rationalized relative to structural influences or other factors.

If desired, the amides in any given peptide can be described experimentally by fitting the HDX profiles to a tri-exponential expression. This involves characterizing all the different amides and their k_{HDX} values via average values according to fast (N_1), medium (N_2) or slow (N_3) [146,161,163]

$$D_t = N_1[1 - e^{-k_1 t}] + N_2[1 - e^{-k_2 t}] + N_3[1 - e^{-k_3 t}]$$

Equation 1.13

However, depending on the kinetic behavior observed, single or double exponential expressions may be suitable as well.

1.5 Scope of Thesis

To better understand effects of oxidative damage, the current work focused on Mb as a simple model protein. We tested the effects of various oxidants including H_2O_2, chloramine-T, and *tert*-butyl hydroperoxide (TBHP) to identify reaction conditions in an effort to produce relatively homogenous reaction products that could then be interrogated by a range of MS-based analytical workflows (including LC-MS/MS, HDX-MS, and IM/MS). TBHP was identified as the most suitable reagent to produce a controlled oxidation product; minimizing unoxidized fraction and products of overoxidation. Previous studies in the literature[165,166] suggested TBHP to be a methionine specific oxidizing agent; however; through the rigorous bottom-up and top-down testing of this project, we debunked this notion.

A key challenge to HDX-MS experiments with oxidized protein is the occurrence of peak broadening and peak splitting. These phenomena interfere with spectral data analysis, as most ROS produce a heterogeneous mix of oxidized proteoforms. For this reason, the application of HDX-MS to oxidized protein has been avoided by other laboratories, leaving a gap of information regarding pathologically relevant systems. This work aims to begin closing existing literature gaps through the rigorous structural analysis of the model protein, Mb, after oxidation. By aiming to overcome the challenges associates with HDX-MS of oxidized samples, this work sheds light upon the efficacy of the method in depicting dynamic alterations, secondary to covalent modification. By demonstrating analyses using a protein that is only specifically modified in a few known sites, further works may assess additive effects of further oxidative-damage events, leading up to the point of aggregation. The combination of various analytical approaches in this work may serve as an outline for further studies on other oxidatively damaged proteins that are relevant for key pathological pathways.

1.6 References

1 A. L. Lehninger, *Biochemistry*, Worth, New York, 2nd ed., 1975.

2 G. Zubay, *Biochemistry*, Wm. C. Brown, Dubuque, IA, 4th edn., 1998.

3 S. Reeg and T. Grune, *Antioxidants Redox Signal.*, 2015, **23**, 239–255.

4 B. S. Berlett and E. R. Stadtman, *J. Biol. Chem.*, 1997, 272, 20313–20316.

5 E. R. Stadtman, *Free Radic. Res.*, 2006, **40**, 1250–1258.

6 R. Tycko, *Protein Sci.*, 2014, **23**, 1528–1539.

7 M. Bucciantini, E. Giannoni, F. Chiti, F. Baroni, L. Formigli, J. Zurdo, N. Taddei, G. Ramponi, C. M. Dobson and M. Stefani, *Nature*, 2002, **416**, 507–511.

8 V. N. Uversky and A. L. Fink, *Protein Rev.*, 2006, 1,2.

9 L. M. Luheshi, D. C. Crowther and C. M. Dobson, *Curr. Op. Chem. Biol.*, 2008, **12**, 25–31.

10 J. X. Pan, J. Han, C. H. Borchers and L. Konermann, *Biochemistry*, 2012, **51**, 3694–3703.

11 R. G. Spiro, *Glycobiology*, 2002, **12**, 43R-56R.

12 G. N. Ramachandran and V. Sasisekharan, *Adv. Protein Chem.*, 1968, **23**, 283–437.

13 L. Pauling, R. B. Corey and H. R. Branson, *Proc. Natl. Acad. Sci.*, 1951, **37**, 205–211.

14 R. B. Corey and L. Pauling, *Proc. R. Soc. London B*, 1953, **141**, 10–20.

15 J. N. Israelachvili, *Q. Rev. Biophys.*, 1974, **6**, 341–387.

16 C. B. Anfinsen, *Science (80-.).*, 1973, **181**, 223–230.

17 G. A. Petsko and D. Ringe, *Protein Structure and Function*, New Science Press Ltd., London, UK, 2004.

18 A. Roy, A. Kucukural and Y. Zhang, *Nat. Protoc.*, 2010, **5**, 725–738.

19 J. Yang, R. Yan, A. Roy, D. Xu, J. Poisson and Y. Zhang, *Nat. Methods*, 2015, **12**, 7–8.

20 J. C. Kendrew, G. Bodo, H. M. Dintzis, R. G. Parrish, H. Wyckoff and D. C. Phillips, *Nature*, 1958, **181**, 662–666.

21 H. Frauenfelder, S. G. Sligar and P. G. Wolynes, *Science (80-.).*, 1991, **254**, 1598–1603.

22 H. Frauenfelder, G. Chen, J. Berendzen, P. W. Fenimore, H. Jansson, B. H. McMahon, I. R. Stroe, J. Swenson and R. D. Young, *Proc. Natl. Acad. Sci. U.S.A.*, 2009, **106**, 5129–5134.

23 S. Hammes-Schiffer, *Biochemistry*, 2013, **52**, 2012–2020.

24 K. Henzler-Wildman and D. Kern, *Nature*, 2007, **450**, 964–972.

25 G. Bhabha, J. Lee, D. C. Ekiert, J. Gam, I. A. Wilson, H. J. Dyson, S. J. Benkovic and P. E. Wright, *Science (80-.).*, 2011, **332**, 234–238.

26 C. M. Venkatachalam, X. Jiang, T. Oldfield and M. Waldman, *J. Mol. Graph. Model.*, 2003, **21**, 289–307.

27 R. Yasuda, H. Noji, K. Kinosita and M. Yoshida, *Cell*, 1998, **93**, 1117–1124.

28 S. Mukherjee, R. P. Bora and A. Warshel, *Q. Rev. Biophys.*, 2015, **48**, 395–403.

29 A. Murcia Rios, S. Vahidi, S. D. Dunn and L. Konermann, *J. Am. Chem. Soc.*, 2018, **140**, 14860–14869.

30 H. Itoh, A. Takahashi, K. Adachi, H. Noji, R. Yasuda, M. Yoshida and K. Kinosita, *Nature*, 2004, **427**, 465–468.

31 M. F. Perutz, G. Fermi, C. Poyart, J. Pagnier and J. Kister, *J. Mol. Biol.*, 1993, **233**, 536–545.

32 M. F. Perutz, E. J. Heidner, J. E. Ladner, J. G. Beetlestone, C. Ho and E. F. Slade, *Biochemistry*, 1974, **13**, 2187–2200.

33 M. F. Perutz, A. J. Wilkinson, M. Paoli and G. G. Dodson, *Annu. Rev. Biophys. Biomol. Struct.*, 1998, **27**, 1–34.

34 T. Yonetani and M. Laberge, *Biochim. Biophys. Acta*, 2008, **1784**, 1146–1158.

35 M. K. Safo and D. J. Abraham, *Biochemistry*, 2005, **44**, 8347–8359.

36 M. A. Sowole, S. A. Simpson, Y. V Skovpen, D. R. J. Palmer and L. Konermann, *Biochemistry*, 2016, **55**, 5413–5422.

37 R. C. Killoran, M. A. Sowole, M. A. Halim, L. Konermann and W.-Y. Choy, *Protein Sci.*, 2016, **25**, 1420–1429.

38 S.-R. Tzeng and C. G. Kalodimos, *Nat. Chem. Biol.*, 2013, **9**, 462–465.

39 R. Nussinov and C. J. Tsai, *Trends Pharmacol. Sci.*, 2014, **35**, 256–264.

40 R. O. Dror, H. F. Green, C. Valant, D. W. Borhani, J. R. Valcourt, A. C. Pan, D. H. Arlow, M. Canals, J. R. Lane, R. Rahmani, J. B. Baell, P. M. Sexton, A. Christopoulos and D. E. Shaw, *Nature*, 2013, **503**, 295-+.

41 F. De Smet, A. Christopoulos and P. Carmeliet, *Nat. Biotechnol.*, 2014, **32**, 1113–1120.

42 H. Sies, *Klin. Wochenschr.*, 1991, **69**, 965–968.

43 E. Birben, U. M. Sahiner, C. Sackesen, S. Erzurum and O. Kalayci, *World Allergy Organ. J.*, 2012, **5**, 9–19.

44 D. J. Betteridge, *Metabolism.*, 2000, **49**, 3–8.

45 M. K. Shigenaga, T. M. Hagen and B. N. Ames, *Proc. Natl. Acad. Sci. U. S. A.*, 1994, **91**, 10771–8.

46 L. de Lucca Camargo and R. M. Touyz, in *Textbook of Vascular Medicine*, Springer International Publishing, Cham, 2019, pp. 127–136.

47 C. C. Winterbourn, A. J. Kettle and M. B. Hampton, *Annu. Rev. Biochem.*, 2016, **85**, 765–792.

48 S. Reuter, S. C. Gupta, M. M. Chaturvedi and B. B. Aggarwal, *Free Radic. Biol. Med.*, 2010, 49, 1603–1616.

49 M. J. Davies, *Biochem. J.*, 2016, 473, 805–825.

50 N. J. Kruger and A. Von Schaewen, *Curr. Opin. Plant Biol.*, 2003, 6, 236–246.

51 X. S. Wang, H. B. Kim, A. Szuchman-Sapir, A. Mcmahon, J. M. Dennis and P. K. Witting, , DOI:10.1016/j.abb.2016.10.013.

52 K. M. Holmström and T. Finkel, *Nat. Rev. Mol. Cell Biol.*, 2014, 15, 411–421.

53 M. Valko, D. Leibfritz, J. Moncol, M. T. D. Cronin, M. Mazur and J. Telser, *Int. J. Biochem. Cell Biol.*, 2007, 39, 44–84.

54 A. Drazic and J. Winter, *Biochim. Biophys. Acta - Proteins Proteomics*, 2014, **1844**, 1367–1382.

55 S. B. Nimse and D. Pal, *Rsc Adv.*, 2015, **5**, 27986–28006.

56 G. Tezel, *Prog. Retin. Eye Res.*, 2006, 25, 490–513.

57 S. Grimm, A. Hoehn, K. J. Davies and T. Grune, *Free Radic. Res.*, 2011, 45, 73–88.

58 M. Rykaer, B. Svensson, M. J. Davies and P. Hä, , DOI:10.1021/acs.jproteome.7b00330.

59 A. M. R. De Graff, M. J. Hazoglou and K. A. Dill, *Structure*, 2016, **24**, 329–336.

60 E. R. Stadtman, *Protein Oxidation and Aging*, 1992, vol. 257.

61 J. Hallwell, Barry; Gutteridge, *Free Radicals in Biology and Medicine*, Oxford University Press, New York, NY, 5th edn., 2015.

62 T. J. A. Höhn and T. Grune, *Redox Biol.*, 2014, **2**, 99–104.

63 C. C. W. Verlackt, W. Van Boxem, D. Dewaele, F. Lemiere, F. Sobott, J. Benedikt, E. C. Neyts and A. Bogaerts, *J. Phys. Chem. C*, 2017, **121**, 5787–5799.

64 E. R. Stadtman and R. L. Levine, *Amino Acids*, 2003, **25**, 207–218.

65 L. Frémont, *Life Sci.*, 2000, **66**, 663–673.

66 M. Jang, L. Cai, G. O. Udeani, K. V Slowing, C. F. Thomas, C. W. Beecher, H. H. Fong, N. R. Farnsworth, A. D. Kinghorn, R. G. Mehta, R. C. Moon and J. M. Pezzuto, *Science (80-.).*, 1997, **275**, 218–20.

67 L. Hung, J.-K. Chen, S.-S. Huang, R.-S. Lee and M.-J. Su, *Cardiovasc. Res.*, 2000, **47**, 549–555.

68 J. A. Baur and D. A. Sinclair, *Nat. Rev. Drug Discov.*, 2006, **5**, 493–506.

69 C. A. de la Lastra and I. Villegas, *Biochem. Soc. Trans.*, 2007, **35**, 1156–60.

70 D. E. Heppner, C. M. Dustin, C. Y. Liao, M. Hristova, C. Veith, A. C. Little, B. A. Ahlers, S. L. White, B. Deng, Y. W. Lam, J. N. Li and A. van der Vliet, *Nat. Commun.*, , DOI:10.1038/s41467-018-06790-1.

71 A. Höhn, J. König and T. Grune, *J. Proteomics*, 2013, **92**, 132–159.

72 K. J. A. Davies, *Biochimie*, 2001, 301–310.

73 P. Ricchiuto, A. V Brukhno and S. Auer, *J. Phys. Chem. B*, 2012, **116**, 5384–5390.

74 K. K. Sharma and P. Santhoshkumar, *Biochim. Biophys. Acta - Gen. Subj.*, 2009, 1790, 1095–1108.

75 J. L. Louie, R. J. Kapphahn and D. A. Ferrington, *Exp. Eye Res.*, 2002, **75**, 271–284.

76 A. Spector, *FASEB*, 1995, **9**, 1173–82.

77 D. Eliezer, J. Yao, H. J. Dyson and P. E. Wright, *Nat. Struct. Biol.*, 1998, **5**, 148–155.

78 D. Eliezer and P. E. Wright, *J. Mol. Biol.*, 1996, **263**, 531–538.

79 P. A. Jennings and P. E. Wright, *Science (80-.).*, 1993, **262**, 892–896.

80 S. Cavagnero, Y. Thériault, S. S. Narula, H. J. Dyson and P. E. Wright, *Protein Sci.*, 2000, **9**, 186–193.

81 E. E. Scott, E. V Paster and J. S. Olson, *J. Biol. Chem.*, 2000, **275**, 27129–27136.

82 S. V Evans and G. D. Brayer, *J. Mol. Biol.*, 1990, **213**, 885–897.

83 A. Ostermann, R. Waschipky, F. G. Parak and G. U. Nienhaus, *Nature*, 2000, **404**, 205–208.

84 M. Schmidt, K. Nienhaus, R. Pahl, A. Krasselt, S. Anderson, F. Parak, G. U. Nienhaus and V. Srajer, *Proc. Nat. Acad. Sci.*, 2005, **102**, 11704–11709.

85 R. S. Johnson and K. A. Walsh, *Protein Sci.*, 1994, **3**, 2411–2418.

86 G. A. Ordway and D. J. Garry, *J. Exp. Biol.*, 2004, **207**, 3441 LP – 3446.

87 J. Pan, J. Han, C. H. Borchers and L. Konermann, *J. Am. Chem. Soc.*, 2009, **131**, 12801–12808.

88 C. Faustman, Q. Sun, R. Mancini and S. P. Suman, *Meat Sci.*, 2010, 86, 86–94.

89 T. Wazawa, A. Matsuoka, G. Tajima, Y. Sugawara, K. Nakamura and K. Shikama, *Biophys. J.*, 1992, **63**, 544–50.

90 M. A. Sowole, S. Vuong and L. Konermann, *Anal. Chem.*, 2015, **87**, 9538–9545.

91 A. J. Szuchman-Sapir, D. I. Pattison, N. A. Ellis, C. L. Hawkins, M. J. Davies and P. K. Witting, *Free Radic. Biol. Med.*, 2008, **45**, 789–798.

92 T. R. n Ulrike B. Hendgen-Cotta, Malte Kelm, *Free Radic. Biol. Med.*, 2014, **73**, 252–259.

93 J. B. Wittenberg and B. A. Wittenberg, *J. Exp. Biol.*, 2003, **206**, 2011 LP – 2020.

94 D. A. Skoog, *Principles of Instrumental Analysis*, Brooks/Cole Thomson Learning, Toronto, 1998.

95 F. C. Strong, *Anal. Chem.*, 1952, **24**, 338–342.

96 S. C. Gill and P. H. von Hippel, *Anal. Biochem.*, 1989, **182**, 319–326.

97 W. Zheng, N. Shan, L. Yu and X. Wang, *Dye. Pigment.*, 2008, **77**, 153–157.

98 S. W. Kelly, T. J. Jess and N. C. Price, *Biochim. Biophys. Acta*, 2005, **1751**, 119–139.

99 S. Kelly and N. Price, *Curr. Protein Pept. Sci.*, 2000, **1**, 349–384.

100 K. Nakanishi, N. Berova and R. W. Woody, *Circular Dichroism*, VCH, New York Weinheim Cambridge, 1994.

101 N. J. Greenfield, *Nat. Protoc.*, 2006, **1**, 2876–2890.

102 J. P. Hennessey and W. C. Johnson, *Biochemistry*, 1981, **20**, 1085–1094.

103 N. V. Bhagavan, *Medical biochemistry*, Harcourt/Academic Press, 2002.

104 W. C. Johnson, *Proteins Struct. Funct. Genet.*, 1990, **7**, 205–214.

105 D. I. Hoult and B. Bhakar, *NMR Signal Reception: Virtual Photons and Coherent Spontaneous Emission*, John Wiley & Sons, Inc. Concepts Magn Reson, 1997, vol. 9.

106 G. Wagner and K. Wüthrich, *J. Mol. Biol.*, 1982, **155**, 347–366.

107 K. Wüthrich, in *Encyclopedia of Life Sciences (www.els.net)*, Nature Pulishing Group, London, 2001.

108 D. S. Wishart, B. D. Sykes and F. M. Richards, *J. Mol. Biol.*, 1991, **222**, 311–333.

109 D. M. Rosenbaum, V. Cherezov, M. A. Hanson, S. G. F. Rasmussen, F. S. Thian, T. S. Kobilka, H. Choi, X. Yao, W. I. Weis, R. C. Stevens and B. K. Kobilka, *Science (80-.).*, 2007, **318**, 1266–1273.

110 B. Domon and R. Aebersold, *Science (80-.).*, 2006, **312**, 212–217.

111 J. B. Fenn, M. Mann, C. K. Meng, S. F. Wong and C. M. Whitehouse, *Science (80-.).*, 1989, **246**, 64–71.

112 B. A. Thomson, *J. Am. Soc. Mass Spectrom.*, 1998, **9**, 187–193.

113 Lord Rayleigh, *Philos. Mag.*, 1882, **14**, 184–186.

114 J. B. Fenn, *Angew. Chem. Int. Ed.*, 2003, **42**, 3871–3894.

115 M. Dole, L. L. Mack, R. L. Hines, R. C. Mobley, L. D. Ferguson and M. B. Alice, *J. Chem. Phys.*, 1968, **49**, 2240–2249.

116 J. V Iribarne and B. A. Thomson, *J. Chem. Phys.*, 1976, **64**, 2287–2294.

117 L. Konermann, E. Ahadi, A. D. Rodriguez and S. Vahidi, *Anal. Chem.*, 2013, **85**, 2–9.

118 P. Kebarle and U. H. Verkerk, *Mass Spectrom. Rev.*, 2009, **28**, 898–917.

119 F. J. de la Mora, *Anal. Chim. Acta*, 2000, **406**, 93–104.

120 H. K. Hustoft, H. Malerod, S. R. Wilson, L. Reubsaet, E. Lundanes and T. Greibrokk, *4 A Critical Review of Trypsin Digestion for LC-MS Based Proteomics*, .

121 J. V Olsen, S. Ong and M. Mann, *Mol. Cell. Proteomics*, 2004, **3**, 608–614.

122 B. F. Shaw, H. Arthanari, M. Narovlyansky, A. Durazo, D. P. Frueh, M. P. Pollastri, A. Lee, B. Bilgicer, S. P. Gygi, G. Wagner and G. M. Whitesides, *J. Am. Chem. Soc.*, 2010, **132**, 17411–17425.

123 D. D. Gouveia, A. M. N. Silva, R. Vitorino, M. Rosário, M. Domingues and P. Domingues, *Eur. J. Mass Spectrom.*, 2014, **20**, 271–278.

124 K. M. Burns, M. Rey, C. A. H. Baker and D. C. Schriemer, *Mol. Cell. Proteomics*, 2013, **12**, 539–548.

125 L. C. Gillet, A. Leitner and R. Aebersold, in *Annu. Rev. Anal. Chem.*, eds. P. W. Bohn and J. E. Pemberton, Annual Reviews, Palo Alto, 2016, vol. 9, pp. 449–472.

126 F. Lanucara and C. E. Eyers, *Mass Spectrom. Rev.*, 2013, **32**, 27–42.

127 W. Cui, H. W. Rohrs and M. L. Gross, *Analyst*, 2011, **136**, 3854–3864.

128 J. Pan and C. H. Borchers, *Proteomics*, 2013, **13**, 974–981.

129 A. B. Kanu, P. Dwivedi, M. Tam, L. M. Matz and H. H. Hill, *J. Mass Spectrom.*, 2008, **43**, 1–22.

130 B. T. Ruotolo, J. L. P. Benesch, A. M. Sandercock, S.-J. Hyung and C. V Robinson, *Nat. Protoc.*, 2008, **3**, 1139–1152.

131 Y. Sun, S. Vahidi, M. A. Sowole and L. Konermann, *J. Am. Soc. Mass Spectrom.*, 2016, **27**, 31–40.

132 C. Eldrid, J. Ujma, S. Kalfas, N. Tomczyk, K. Giles, M. Morris and K. Thalassinos, *Anal. Chem.*, 2019, **91**, 7554–7561.

133 J. Ujma, D. Ropartz, K. Giles, K. Richardson, D. Langridge, J. Wildgoose, M. Green and S. Pringle, *J. Am. Soc. Mass Spectrom.*, 2019, **30**, 1028–1037.

134 J. L. Wildgoose, K. Giles, S. D. Pringle, S. Koeniger, S. J. Valentine, R. H. Bateman

and D. E. Clemmer, in *Proc. 54th ASMS Conference on Mass Spectrometry & Allied Topics*, ASMS, Seattle, WA, May 28–June 1st, 2006.

135 S. M. Stow, T. J. Causon, X. Y. Zheng, R. T. Kurulugama, T. Mairinger, J. C. May, E. E. Rennie, E. S. Baker, R. D. Smith, J. A. McLean, S. Hann and J. C. Fjeldsted, *Anal. Chem.*, 2017, **89**, 9048–9055.

136 C. A. Scarff, K. Thalassinos, G. R. Hilton and J. H. Scrivens, *Rapid Commun. Mass Spectrom.*, 2008, **22**, 3297–3304.

137 P. Liuni, B. Deng and D. J. Wilson, *Analyst*, 2015, **14**, 6973–6979.

138 J. P. Williams, J. A. Lough, I. Campuzano, K. Richardson and P. J. Sadler, *Rapid Commun. Mass Spectrom.*, 2009, **23**, 3563–3569.

139 K. Giles, J. P. Williams and I. Campuzano, *Rapid Commun. Mass Spectrom.*, 2011, **25**, 1559–1566.

140 J. J. Englander, C. Del Mar, W. Li, S. W. Englander, J. S. Kim, D. D. Stranz, Y. Hamuro and V. L. Woods, *Proct. Nat. Acad. Sci.*, 2003, **100**, 7057–7062.

141 G. F. Pirrone, R. E. Iacob and J. R. Engen, *Anal. Chem.*, 2015, **87**, 99–118.

142 A. Hvidt and K. Linderstrom-Lang, *Biochem. Biophys. Acta*, 1954, **14**, 574–575.

143 K. Linderstrøm-Lang, in *Symposium on Protein Structure*, ed. A. Neuberger, Methuen & CO LTD, London, 1958, pp. 23–34.

144 S. W. Englander, L. M. Bai and T. R. Sosnick, *Protein Sci.*, 1997, **6**, 1101–1109.

145 S. W. Englander, T. R. Sosnick, J. J. Englander and L. Mayne, *Curr. Opin. Struct. Biol.*, 1996, **6**, 18–23.

146 G. Wagner and K. Wüthrich, *Methods Enzymol.*, 1986, **131**, 307–326.

147 L. Konermann, J. Pan and Y. H. Liu, *Chem. Soc. Rev.*, 2011, **40**, 1224–1234.

148 L. Konermann, X. Tong and Y. Pan, *J. Mass Spectrom.*, 2008, **43**, 1021–1036.

149 T. E. Wales and J. R. Engen, *Mass Spectrom. Rev.*, 2006, **25**, 158–170.

150 D. D. Weis, T. E. Wales, J. R. Engen, M. Hotchko and L. F. Eyck, *J. Am. Soc. Mass Spectrom.*, 2006, **17**, 1498–1509.

151 J. Zhang, P. Ramachandran, R. Kumar and M. L. Gross, *J. Am. Soc. Mass Spectrom.*, 2013, **24**, 450–453.

152 Y. Deng, Z. Zhang and D. L. Smith, *J. Am. Soc. Mass Spectrom.*, 1999, **10**, 675–684.

153 B. T. Walters, A. Ricciuti, L. Mayne and S. W. Englander, *J. Am. Soc. Mass Spectrom.*, 2012, **23**, 2132–2139.

154 K. Dharmasiri and D. L. Smith, *Anal. Chem.*, 1996, **68**, 2340–2344.

155 Z. Zhang and D. L. Smith, *Protein Sci.*, 1993, **2**, 522–531.

156 Y. Bai, J. S. Milne, L. Mayne and S. W. Englander, *Proteins Struct., Funct., Genet.*, 1993, **17**, 75–86.

157 J. D. Venable, L. Okach, S. Agarwalla and A. Brock, *Anal. Chem.*, 2012, **84**, 9601–9608.

158 D. L. Smith, Y. Deng and Z. Zhang, *J. Mass Spectrom.*, 1997, **32**, 135–146.

159 L. Swint-Kruse and A. D. Robertson, *Biochemistry*, 1996, **35**, 171–180.

160 N. L. Kelleher, H. Y. Lin, G. A. Valaskovic, D. J. Aaserud, E. K. Fridriksson and F. W. McLafferty, *J. Am. Chem. Soc.*, 1999, **121**, 806–812.

161 J. Liu and L. Konermann, *J. Am. Soc. Mass Spectrom.*, 2009, **20**, 819–828.

162 A. J. Percy, M. Rey, K. M. Burns and D. C. Schriemer, *Anal. Chim. Acta*, 2012, **721**, 7–21.

163 G. R. Masson, J. E. Burke, N. G. Ahn, G. S. Anand, C. Borchers, S. Brier, G. M. Bou-Assaf, J. R. Engen, S. W. Englander, J. Faber, R. Garlish, P. R. Griffin, M. L. Gross, M. Guttman, Y. Hamuro, A. J. R. Heck, D. Houde, R. E. Iacob, T. J. D. Jørgensen, I. A. Kaltashov, J. P. Klinman, L. Konermann, P. Man, L. Mayne, B. D. Pascal, D. Reichmann, M. Skehel, J. Snijder, T. S. Strutzenberg, E. S. Underbakke, C. Wagner, T. E. Wales, B. T. Walters, D. D. Weis, D. J. Wilson, P. L. Wintrode, Z. Zhang, J. Zheng, D. C. Schriemer and K. D. Rand, *Nat. Methods*, 2019, **16**, 595–602.

164 D. D. Weis, *Hydrogen exchange mass spectrometry of proteins : fundamentals, methods, and applications*, John Wiley & Sons, 2016.

165 M. Imiołek, G. Karunanithy, W.-L. Ng, A. J. Baldwin, V. Gouverneur and B. G. Davis, *J. Am. Chem. Soc.*, 2018, **140**, 1568–1571.

166 R. G. Keck, *Anal. Biochem.*, 1996, **236**, 56–62.

167 W. E. Balch, R. I. Morimoto, A. Dillin and J. W. Kelly, *Science (80-.).*, 2008, **319**, 916–919.

168 A. G. Madian and F. E. Regnier, *J. Proteome Res.*, 2010, **9**, 3766–3780.

169 P. R. Angelova and A. Y. Abramov, *FEBS Lett.*, 2018, **592**, 692–702.

170 I. Verrastro, S. Pasha, K. T. Jensen, A. R. Pitt and C. M. Spickett, *Biomolecules*, 2015, 5, 378–411.

171 B. Halliwell and M. Whiteman, *Br. J. Pharmacol.*, 2004, **142**, 231–255.

172 H. Mirzaei and F. Regnier, *J. Chromatogr. A*, 2006, **1134**, 122–133.

173 M. J. Davies, *Biochim. Biophys. Acta - Proteins Proteomics*, 2005, **1703**, 93–109.

174 I. Dalle-Donne, R. Rossi, D. Giustarini, A. Milzani and R. Colombo, *Clin. Chim. Acta*, 2003, 329, 23–38.

175 X. Li, Z. Li, B. Xie and J. S. Sharp, *J. Am. Soc. Mass Spectrom.*, 2013, **24**, 1767–1776.

176 E. Shacter, *Drug Metab. Rev.*, 2000, **32**, 307–326.

177 M. Karplus and J. A. McCammon, *Ann. Rev. Biochem.*, 1983, **53**, 263–300.

178 L. Konermann, J. Pan and Y. H. Liu, *Chem. Soc. Rev.*, 2011, **40**, 1224–1234.

179 L. Konermann, S. Vahidi and M. A. Sowole, *Anal. Chem.*, 2014, **86**, 213–232.

180 M. Imiołek, G. Karunanithy, W.-L. Ng, A. J. Baldwin, V. Gouverneur and B. G. Davis, , DOI:10.1021/jacs.7b10230.

181 R. Hutchins, M. Hutchins and B. Trost, *Comprehensive organic synthesis: Reduction of C=X to CH2 by Wolff-Kishner and Other Hydrazone Methods*, 8th edn., 1991.

182 G. Schneider and G. A. Sprenger, *Enzym. Kinet. Mech.*, 2003, 197–201.

183 T. Matsui, S. Ozaki and Y. Watanabe, *J. Am. Chem. Soc.*, 1999, **121**, 9952–9957.

184 V. Yin, G. S. Shaw and L. Konermann, *J. Am. Chem. Soc.*, 2017, **139**, 15701–15709.

185 V. Yin, S. H. Mian and L. Konermann, *Chem. Sci.*, , DOI:10.1039/C8SC03624A.

186 R. G. Keck, *Anal. Biochem.*, 1996, **236**, 56–62.

187 C. Giulivi and K. J. Davies, *J. Biol. Chem.*, 2001, **276**, 24129–36.

188 D. Tew and P. R. Ortiz De Montellano, *J. Biol. Chem.*, 1988, **263**, 17880–17886.

189 A. Bachi, I. Dalle-Donne and A. Scaloni, *Chem. Rev.*, 2013, **113**, 596–698.

190 D. D. Gouveia, A. M. N. Silva, R. Vitorino, M. R. M. Domingues and P. Domingues, *Eur. J. Mass Spectrom.*, 2014, **20**, 271–278.

191 P. Wood, Humana Press, New York, NY, 2017, pp. 229–232.

192 O. H. Wheeler and O. Rosado-Lojo, *Tetrahedron*, 1962, **18**, 477–482.

193 D. A. Polasky, F. Lermyte, M. Nshanian, F. Sobott, P. C. Andrews, J. A. Loo and B. T. Ruotolo, *Anal. Chem*, 2018, **90**, 2756–2764.

194 D. A. Polasky, F. Lermyte, M. Nshanian, F. Sobott, P. C. Andrews, J. A. Loo and B. T. Ruotolo, *Anal. Chem.*, 2018, **90**, 2756–2764.

2 Analysis of Oxidatively Modified Myoglobin by Complementary Mass Spectrometry Techniques

2.1 Introduction

As humans and other organisms age, oxidatively damaged proteins can accumulate in the body as the result of encounters with ROS. Oxidative damage contributes to a range of age-related pathologies, as modified proteins may exhibit impaired function.[1–4] This poses particular risks to tissues where proteins are not continuously regenerated. The brain is especially susceptible to oxidative damage due to its high demand for oxygen, leading to various pathologies as discussed in chapter 1.1.3.[5]

Protein oxidation (in particular, carbonyl formation) has long been viewed as a hallmark for measuring the extent of oxidative stress and damage to cells.[6–11] Quantification can be achieved through a variety of methods such as OxyBlots, derivatization with 2,4-dinitrophenylhydrazine, antibody tagging, and covalent labelling with reagents such as Girard's reagent and biotin hydrazide.[8,9,12,13] Alternatively, MS lends itself as an exceptionally sensitive tool for the identification and quantification of oxidative modifications. As outlined in Chapter 1, protein function is governed by protein structure and dynamics.[14–17] Studying the effects of oxidative damage on protein structural dynamics is therefore imperative for the development of treatments to combat oxidation-induced pathologies.

MS offers a number of avenues to probe protein oxidation. Traditional LC-MS/MS bottom-up workflows are widely used, but they may yield incomplete information due to protease inefficiency as a result of oxidative modifications. Top-down MS can potentially overcome this hurdle, yielding residue-resolved information regarding the exact nature of oxidation events. IM-MS can provide additional insight, probing the effects of oxidative modifications on the gas phase structures (CCS) of proteins. Of particular interest is the ability to acquire information on conformational dynamics with high spatial resolution by using HDX-MS.[18–20] Surprisingly, this particular technique is under-utilized when it comes to the characterization of oxidatively modified proteins. Possible reasons for the scarcity of HDX-MS data in this context include the complexity of the samples, as well as the cumbersome data analysis and sample conditioning. The current work aims to overcome some of these complications in pursuit of comprehensive protein analysis.

As discussed in 1.1.3, protein oxidative damage typically results from oxygen-based radicals and other ROS. One of the main biological sources of radicals is the production of hydroxyl radical by metal catalyzed oxidation of H_2O_2, otherwise known as Fenton Chemistry (Scheme 1, below).[21–23] Heme proteins such as Mb, hemoglobin and various cytochromes can be the source of the $Fe^{2+}/^{3+}$ required for these processes.

$$Fe^{2+} + H_2O_2 \rightarrow Fe^{3+} + HO^{\bullet} + HO^{-}$$

$$Fe^{3+} + H_2O_2 \rightarrow Fe^{2+} + HOO^{\bullet} + H^{+}$$

$$2H_2O_2 \rightarrow HO^{\bullet} + HOO^{\bullet} + H_2O$$

Scheme 1: *Formation of oxygen-based radicals from H_2O_2 via Fenton Chemistry.*

The high second order reaction constants for the reaction of peroxide radicals with protein side chains results in low specificity and reproducibility, because the ROS produced in this way cause a wide range of different protein modifications.[10,23] The non-uniform and highly heterogeneous nature of the oxidation products generated by these processes makes their analytical characterization very difficult. For initial method development, it would be desirable to use an oxidant that is more targeted and that produces relatively homogeneous oxidation products. For this reason, we did not focus our attention on H_2O_2, but instead explored alternative options.

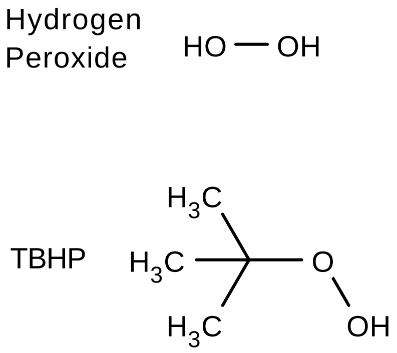

Figure 1: *Chemical structure of hydrogen peroxide (top) and tert-Butyl hydroperoxide (TBHP - bottom)*

TBHP (Figure 1) has been reported by Keck to be a methionine-specific oxidizing agent, targeting solvent exposed methionine residues in native recombinant interferon γ (rIFN-γ) and recombinant tissue-type plasminogen activator (rt-PA).[24] Similarly, experiments by Imiołek et *al.* on Mb yielded promising results that indicated specific methionine oxidation by TBHP.[25] Similar to H_2O_2, TBHP is susceptible to oxy and peroxide radical formation *via* Fenton chemistry. $(CH_3)_3COO^{\bullet}$ and $(CH_3)_3CO^{\bullet}$ can be produced *in situ* at heme iron centers as outlined below:

$$\begin{array}{c} Fe^{2+} + (CH_3)_3COOH \rightarrow Fe^{3+} + (CH_3)_3CO^{\bullet} + HO^{-} \\ Fe^{3+} + (CH_3)_3COOH \rightarrow Fe^{2+} + (CH_3)_3COO^{\bullet} + H^{+} \\ \hline 2\,(CH_3)_3COOH \rightarrow (CH_3)_3CO^{\bullet} + (CH_3)_3COO^{\bullet} + H_2O \end{array}$$

Scheme 2: *Formation of oxygen-based radicals from TBHP via Fenton Chemistry.*

Due to the inherent steric obstruction of tert-butoxyl radicals, second order rate constants are lower than those of hydroxyl radicals, thereby promoting the formation of oxidation patterns that are more straightforward. The reported selectivity and reproducibility of TBHP [24,25] makes this reagent a promising model compound for the experiments of this work, and it was therefore used in our experiments for inducing protein oxidative modifications.

Instead of studying actual *in vivo* protein oxidation, the current work employed Mb as a model system to examine the effects of TBHP exposure *in vitro*. We relied on the presence of heme iron in Mb to induce Fenton chemistry which causes oxidative damage of the protein. The oxidized Mb generated in this way then served as a testbed to adapt and optimize a comprehensive set of MS-based workflows for characterizing the effects of protein oxidation in solution and in the gas phase.

2.2 Methods

2.2.1 Materials

BioUltra ≥ 98% (SDS-PAGE) hMb from equine skeletal muscle, Luperox® TBH70X (*tert*-Butyl hydroperoxide solution – TBHP), Girard's Reagent T (GRT, carboxymethyl-trimethylammonium-hydrazide chloride), and D_2O were sourced from Sigma Aldrich (St. Louis, MO). HCl was purchased from Caledon (Georgetown, ON, Canada). LC-MS grade H_2O was acquired from Optima (Fair Lawn, NJ). Trypsin Gold, mass spectrometry grade, was obtained from Promega (Madison, WI). All pH values were measured with a Fisher (Waltham, MA) AB15 pH meter.

2.2.2 Protein Oxidation

Each TBHP-oxidized protein sample was prepared by creating a solution containing 100 μM myoglobin, 40 mM pH 6.0 ammonium acetate buffer and 2500 μM TBHP oxidant. The samples were immediately placed on ice once mixed and left to react for 60 minutes, in accordance with reference 25.[25] The reaction was quenched by dialysis in 10 kDa MWCO filters via a 13 g, 15-minute centrifugal spin-down, repeated three times. Control protein was prepared under identical conditions, except an equivalent volume of water was added in place of TBHP oxidant.

2.2.3 Isotopic Modelling

Protein Prospector is a software package created by the University of California at San Francisco where isotopic mass distributions are calculated based on chemical composition. Theoretical mass distributions were normalized and plotted against experimental data to model spectra accordingly.

2.2.4 Tryptic Digestion

Digestion samples were prepared using Trypsin Gold, 20% acetonitrile, pH 7.7 ammonium bicarbonate 12.5mM, and 1:20 protein:protease, incubated at 37ºC for 24h. The samples were quenched with 2.5% formic acid. Waters reverse phase nanoACQUITY UPLC separation employed a BEH 1.7 μm, 1 × 100 mm C_{18} column, prior to MS/MS (MS^E) analysis. Waters ProteinLynx Global SERVER is the main data interpretation suite for Waters instruments and was used to decipher and match MS^E data to database values for tryptic myoglobin peptides, where covalent protein modifications can be accounted for. All LC-MS peaks were then manually analyzed to confirm any reported peptides to avoid false positives and negatives.

2.2.5 Covalent Labelling of Oxidatively Modified Protein

Control and oxidized protein stocks were added to a 400 μL solution containing 80 mM of Girard’s reagent T (GRT), 10 μM protein, and 50 mM pH 7.4 phosphate buffer. The samples were incubated at room temperature overnight. To affix the GRT tag, the hydrazone bond was reduced using excess sodium borohydride on ice for 1 h.[26,27] Following, the reaction was quenched by dialysis in 10 kDa MWCO filters via a 13 g, 15-minute centrifugal spin-down repeated three times.

2.2.6 Top-Down CID-IM-MS

Experiments were performed on a Synapt G2-Si ESI quadrupole-time-of-flight instrument set to resolution mode. The instrument parameters were set as follows: cone voltage 20 V, ESI voltage 2.8 kV, source temperature 80 ºC and desolvation temperature 250 ºC. 10 μM protein samples were prepared in 50:50 H_2O:ACN with 0.1% formic acid, and infused directly by way of a syringe pump, flowing at 5 μL/min. MS/MS experiments by collision-induced-dissociation (CID) utilized argon collision gas using 27 V to fragment quadrupole-selected 25+ protein ions. IMS separation following fragmentation was performed in N_2 buffer gas with corresponding wave velocity of 350 m s^{-1} and wave height of 13 V.

2.2.7 HDX/MS

A 1000 μL HDX samples were prepared containing 89% v/v D_2O, 50 mM potassium-phosphate buffer and 5 μM protein. 100 μL aliquots were taken from this stock at specific time intervals and quenched in sample tubes containing chilled hydrochloric acid to a predetermined pH of 2.5 and immediately flash frozen in liquid nitrogen. m_0 samples were used to present a baseline for deuterium uptake by exposing the protein to deuterium buffer under pre-quenched conditions. These samples were created mimicking the composition of prior 100 μL aliquot time interval samples, in that m_0 samples were composed of 89% v/v D_2O, 5 μM protein, 50 mM potassium-phosphate buffer and sufficient hydrochloric acid to reach pH 2.5. m_{100} samples, which represent fully deuterated protein, were left to incubate overnight at 40 °C. At pH 2.5, m_{100} samples represent maximum experimental uptake of denatured protein.

Prior to injection, each frozen sample was rapidly thawed to ~ 0 ºC. Bottom-up HDX-MS was performed using a nanoACQUITY UPLC equipped HDX Manager, mated to a Synapt G2 ESI quadrupole-time-of-flight mass spectrometer (Waters, Milford, MA). Online digestion was performed at 15 ºC using a 2.1 mm × 30 mm POROS pepsin column (Life Technologies/Applied Biosystems, Carlsbad, CA). After passing into the 0 ºC HDX chamber, the eluent becomes trapped on a BEH C_{18}, 1.7 μm, 2.1 × 5 mm guard column. For desalting and peptide separation, a 20 min water/acetonitrile (0.1% formic acid) gradient through a reverse-phase BEH 1.7 μm, 1 × 100 mm C_{18} column was employed. The instrument parameters were set as follows: cone voltage 20 V, electrospray voltage 3 kV, source temperature 80 ºC and desolvation temperature 250 ºC.

MS^E data processing and peptide identification were preformed through Waters PLGS 2.4.3. Peptide matches were manually vetted to ensure accuracy before employing Waters

DynamX 3.0 for analysis of HDX profiles. All experiments were performed in triplicates but due to the nature of some oxidized samples, a few time points were poorly matched by DynamX and deemed extraneous. Error bars are representative of the standard deviation between replicates.

2.2.8 Collision Induced Unfolding - IMS

Experiments were performed on a Synapt G2-Si ESI quadrupole-time-of-flight instrument set to sensitivity mode. The instrument parameters were set as follows: cone voltage 5 V, electrospray voltage 2.8 kV, source temperature 25 ºC and desolvation temperature 40 ºC. 10 μM protein samples were prepared in pH 7.4, 10 mM ammonium acetate, and infused directly by a syringe pump, flowing at 5 μL/min. IMS was performed in N_2 buffer gas with corresponding wave velocity of 350 m s^{-1} and wave height of 13 V. CCS values were calibrated using a mix of denatured and collisionally activated proteins in 49:49:2 (v/v/v) methanol/water/acetic acid.[28] CCS were recorded for the native 9+ protein ion. Collision energy (using argon gas) was incrementally increased stepwise beginning at 0 V, proceeding through default instrument settings of 4 V trap and transfer and increasing steadily inside of a resolvable IMS range.

2.2.9 Collision Induced Dissociation

Experiments were performed on a Synapt G2-Si ESI quadrupole-time-of-flight instrument set to sensitivity mode. The instrument parameters were set as follows: cone voltage 5 V, electrospray voltage 2.8 kV, source temperature 25 ºC and desolvation temperature 40 ºC. 10 μM protein samples were prepared in pH 7.4, 10 mM ammonium acetate, and infused directly by way of a syringe pump, flowing at 5 μL/min. Native 9+ protein ions were quadrupole-selected and subjected to incrementally increasing collisional energy inside the trap cell. Transfer collision energy was held constant at 4 V for every measurement outside of the initial step where all collision energy was turned to 0 V.

2.3 Results and Discussion

2.3.1 Oxidation of Myoglobin

Fenton chemistry is a common *in vivo* and *in vitro* oxidation mechanism, where iron ions catalyze the formation of highly reactive oxygen-based radicals from peroxides (Schemes 1, 2).[3,6,9,10,23] In heme-containing proteins such as myoglobin, hemoglobin, and cytochrome *c*, iron from the porphyrin ring can catalyze these processes.[29–38]

The initial goal of this work was to create a workflow that would generate Mb oxidation products that would be relatively simple to characterize. Our primary aim was to attain full conversion to oxidized species, and secondly, minimize side reactions such that relatively homogeneous oxidation products would be obtained. Hydrogen peroxide (H_2O_2) is a well-established oxidizing reagent; however, the high second order rate constant causes very low selectivity, increasing the complexity of the resultant products.[23,39–43] Hence, after acquiring some preliminary data (not shown) we abandoned the use of H_2O_2 for the current work. Next, we tested chloramine-T as an oxidizing agent. However, problems were encountered with this reactant as well; we could not attain full conversion to oxidized protein without incurring overoxidation and numerous different peaks (data not shown). Ultimately, we settled on TBHP. This oxidant proved most effective in reproducible Mb oxidation, achieving a high level of conversion while avoiding overoxidation. TBHP oxidation of Mb resulted in mass distributions that were dominated by one prominent peak (Figure 2B, Peak 2) with two lower-abundance subspecies (annotated as Peaks 1 and 3 in Figure 2B). The notations “Peak 1”, “Peak 2”, and “Peak 3” will be used throughout the text to identify which species is being referenced. Without proper scrutiny, it would appear that oxidation with TBHP did not achieve full conversion, as a seemingly unoxidized fraction remained in the spectrum (Peak 1). However, closer inspection and isotopic modelling showed that Peak 1 is actually shifted -2 Da relative to the unmodified protein. Fine isotopic structure overlap comparing Peak 1 to unoxidized control myoglobin (Figure 2C) accentuates the difference between the two species.

A -2 Da mass shift could be the result of disulfide bond formation, carbonylation of alcohols, dityrosine formation, or a combination of two -1 Da lysine carbonylation events.[9,39,42–44] All of these outcomes were initially considered; however, since equine skeletal myoglobin contains no cysteine, disulfide bond formation is impossible. Similarly, the presence of only a single tyrosine (Y103) precludes the formation of dityrosine.[45]

Peak 2 was shifted +14 Da relative to control. Although unlikely by Fenton-based TBHP oxidation,[9,39] +14 Da modifications could result from aliphatic carbonylation at leucine, alanine and valine residues, or oxidation of tryptophan to oxolactone.[46] Considering the low likelihood of +14 Da covalent modification, it is more probable that Peak 2 is composed of the modifications causing the -2 Da shift in Peak 1 and a more common +16 Da modification (e.g., at methionine, tyrosine, or tryptophan). Peak 3 is the culmination of further +16 Da and -1 Da modifications, relative to Peak 2. Peak 3 and additional peaks are too low abundance and too broad for accurate characterization at this time, so the main focus of this work remained on Peaks 1 and 2.

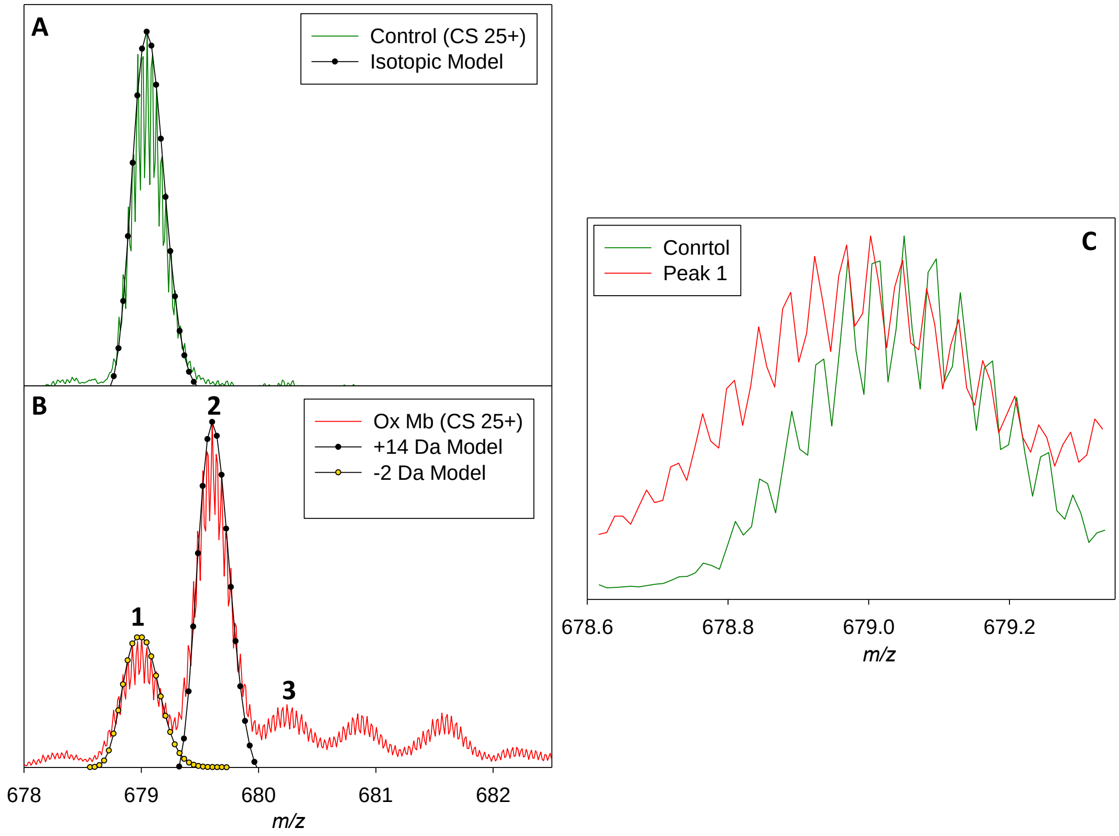

Figure 2: *A) Mass spectrum of unmodified Mb, with overlaid isotopic model, CS 25+. B) Mass spectrum of TBHP-oxidized Mb. The spectrum shows three main peaks (1, 2, 3), dominated by a +14 Da species (Peak 2). Peak 1 corresponds to a -2 Da shift. C) Overlay of isotopic structure of unoxidized (control) Mb, and Peak 1 of oxidized Mb.*

The occurrence of Fenton chemistry under the conditions used here implies that reactive radicals will be created adjacent to the heme group. For this reason, residues close to heme are most likely to experience covalent modification. The most probable amino acids to be oxidized based on proximity to heme and propensity of oxidation are highlighted in Figure 3.[9] These include Tyr103, and Lys96. Other residues non-proximal to heme that readily oxidize are also highlighted.[9] These residues are Lys 56, Lys 102, Met55, Met131, Trp7, and Trp14.

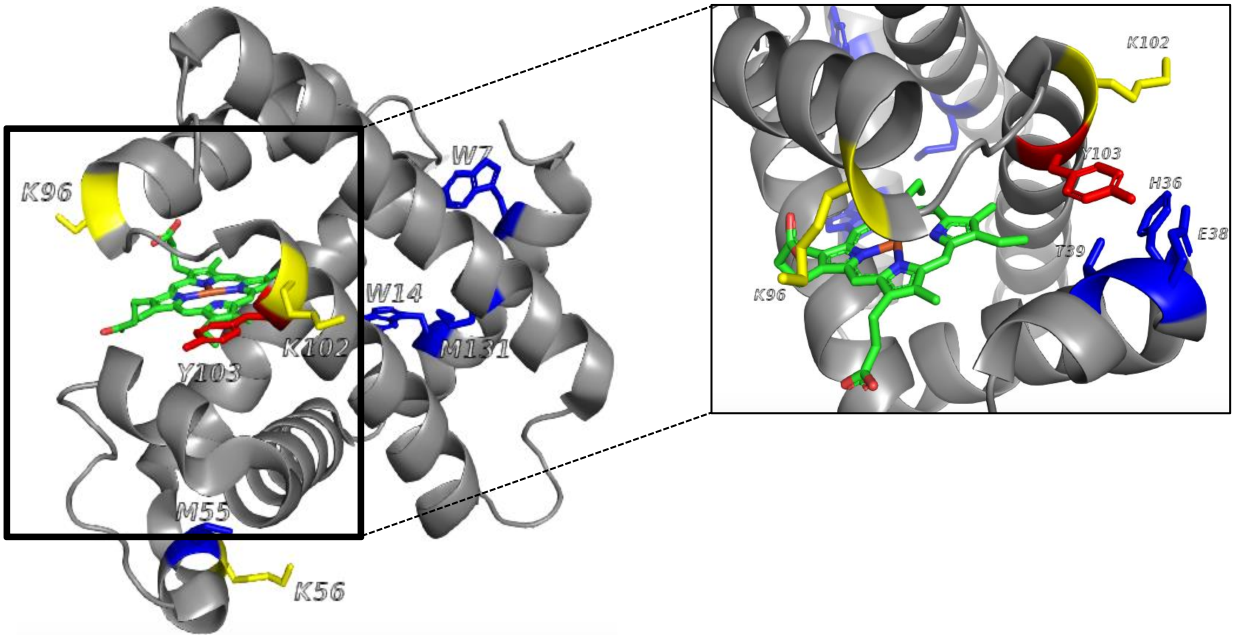

Figure 3: *X-Ray crystal structure of Mb (pdb code 1wla). Residues in close proximity to heme that are likely to be oxidized. The zoomed in panel on the right highlights the proximity of heme to K96 and Y103, as well as proximity of Y103 to peptide 30-40. Colours are used to indicate sites of interest. Yellow: potential sites of -1 Da Lys oxidation. Red: site of +16 Da Tyr-oxidation. Blue: other residues of various interests i.e., potential oxidation targets (pictured left), spatial proximity to oxidized sites (pictured right).*

Even without a detailed analysis of oxidation sites, the mass distributions seen in Figure 2, contain at least three reaction products, clearly highlighting the fact that Mb oxidation by TBHP is *not* a simple process that only affects Met residues (Mb possesses two Met in positions M55 and M131). The unexpected complex oxidation pattern seen here is in stark contrast to the findings of references 24 and 25, which painted a much simpler picture. Additional complexities became apparent when analyzing the mass distributions of the oxidized protein under denaturing ESI conditions. Traditional ESI-MS analyses commonly assume that all charge states under these conditions represent the same mass distribution.[47] Surprisingly, the samples studied here show a very different behavior. To assess the sample variability over different charge states, Figure 4A overlays all charge states in the ESI spectrum of TBHP-oxidized Mb. For higher charge states, the abundance of Peaks 1 and 3 is increased relative to Peak 2. Furthermore, low charge states appear shifted to the left, indicating the possibility of additional oxidative modifications. Figure 4B averages all the spectra derived from the individual charge states and produces an overall distribution that still shows Peak 2 as the most abundant signal with a mass increase of roughly +14 Da. Lower charge states show increasing extent of lysine oxidation (-1 Da) and therefore appear slightly left shifted. The higher charge states show very similar, overlapped mass profiles. The intensity of Peak 2 begins to decrease relative to Peaks 2 and 3, as charge state decreases.

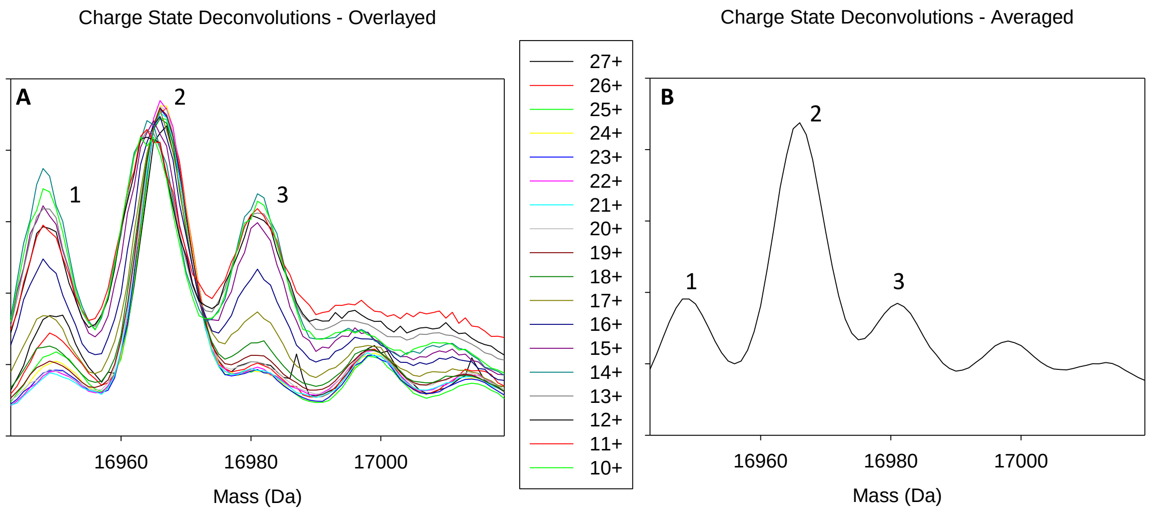

Charge State Deconvolutions - Overlayed

Charge State Deconvolutions - Averaged

Figure 4: *A) Deconvoluted mass distributions of various Mb charge states plotted on a mass axis. B) Average mass distribution generated by summing the data from panel A. Peak 1 averages to a roughly -2 Da shift, and Peak 2 averages to about +14 Da, relative to the unmodified control.*

2.3.2 Characterization of Oxidative Modifications by Bottom-Up MS

Being the gold standard of bottom-up proteomics, trypsin digestion is often the first step in identifying covalent modifications. Both the control (Figure 5A) and oxidized (Figure 5B) were digested under identical conditions but produced different LC chromatograms. Trypsin selectively cleaves after arginine and lysine due to their positive charge; if these sites become modified and lose their intrinsic charge, the enzyme will not cleave.[48] Figure 5 highlights the significant depletion of two peptides, 97-102 and 103-118, and minor depletion of 51-56, suggesting covalent modification of lysines K56, K96 and K102. This assay was unable to confirm the presence of lysine modifications as the corresponding missed-cleaved peptides were not apparent. Due to peak broadening in the oxidized chromatogram, data analysis software PLGS (Waters) and PEAKS (BSI) returned many false-positives and inaccurate sequence coverage. This prompted us to perform manual analyses of all the spectra. The emergence of a new chromatographic peak raised the possibility of incomplete digestion due to protein aggregation and/or crosslinked products as the MS and MS/MS data did not match any known or modified Mb peptide, even when using de novo workflows. We found no modification at either methionine (M55 and M131), thereby debunking previous claims by Imiołek et *al. (see their Figure S8c)*[25] regarding the purported selectivity of TBHP toward methionine under the exact conditions used in this experiment. Similarly, Keck[24] had claimed that TBHP would specifically oxidize surface methionine residues although that author did not use Mb for his study. Our results did not uncover any +14 Da or +16 Da modified peptides, even with ~95% coverage of the oxidize protein. This suggests that the main modifications comprising Peak 2 must be located within the residues that were not covered in our experiments (97-102) or the peptides that were significantly depleted (51-56, 97-102, 103-118).

Alternative proteases including Glu-C and chymotrypsin were also used in an attempt to further characterize oxidized Mb samples but resulted in far worse coverage and no additional information relative to trypsin alone.

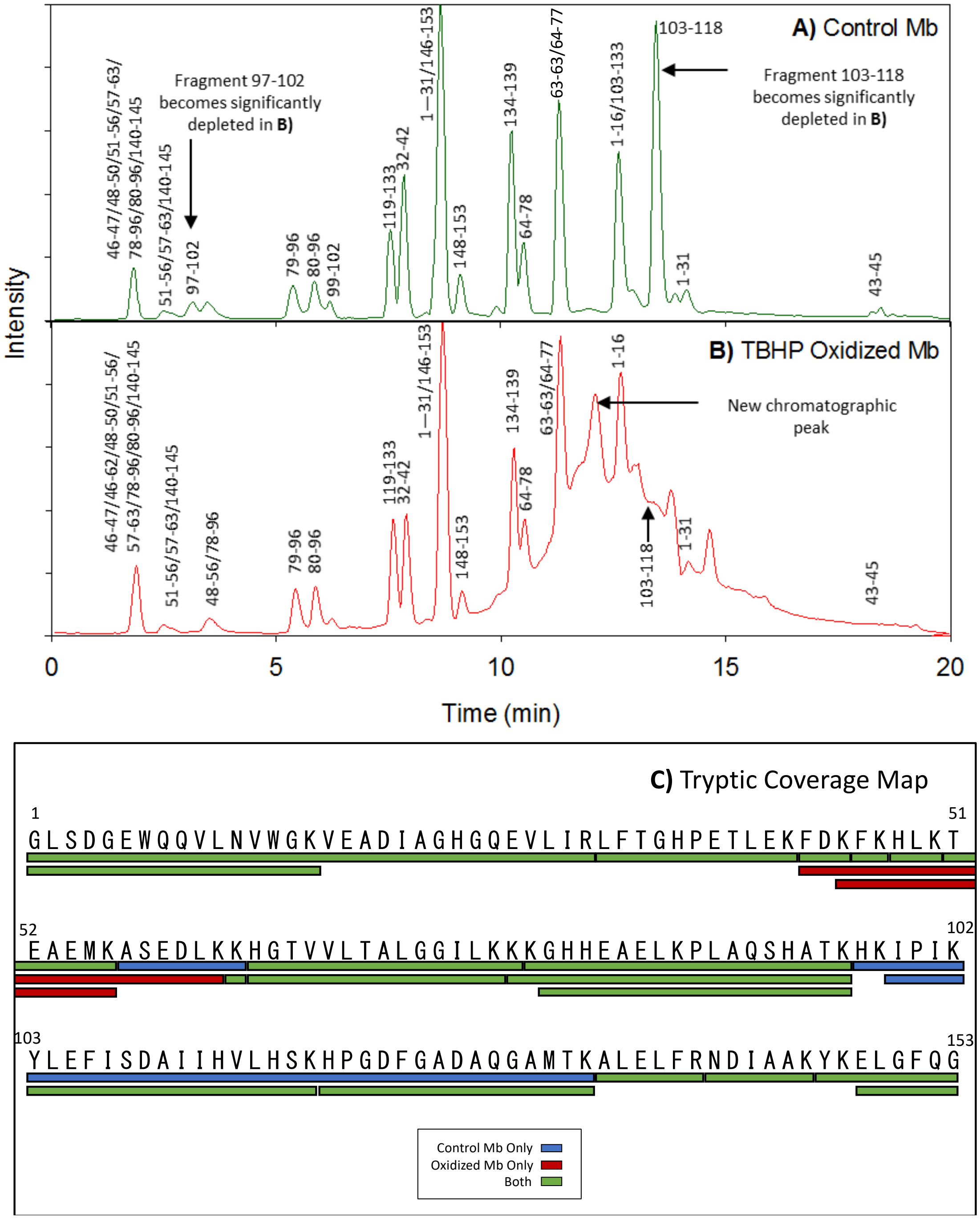

Figure 5: *A) LC/MS total ion chromatogram of a Mb tryptic digest (unmodified control), displaying complete digestion and 100% coverage. B) LC/MS total ion chromatogram of a Mb digest after oxidizing the protein with TBHP. Note the reduced digestion efficiency. Tryptic peptides 97-102 and 103-118 show significant depletion after oxidation - indicating oxidative modifications in those regions. C) Tryptic peptide coverage map.*

2.3.3 Covalent Labelling of Oxidized Mb with GRT

To test the possibility of lysine carbonylation to aminoadipic semialdehyde, covalent labelling with Girard's reagent T (GRT) was used. GRT labelling forms products with a distinct mass shift of +116 Da (after reduction of the imine double bond).[26,27,49,50] Figure 6A shows the absence of GRT labels on unoxidized control Mb, after sufficient exposure. Figure 6B shows the TBHP-oxidized Mb sample prior to any GRT exposure. Figure 6C confirms the presence of carbonylated species present in Peaks 2 and 3, as resultant GRT-tagged species appear +116 Da downstream once oxidized Mb is sufficiently exposed to GRT. The GRT tagged peaks that resulted from Peak 1 covalent labelling unfortunately became shadowed by the heightened baseline. Peaks 1 and 2 appeared significantly depleted and shifted by +2 Da, confirming that most of the species composing these peaks were lysine carbonylated. This pattern also reaffirms our initial suspicion that Peak 2 comprises a +16 Da oxidation instead of a genuine +14 Da modification.

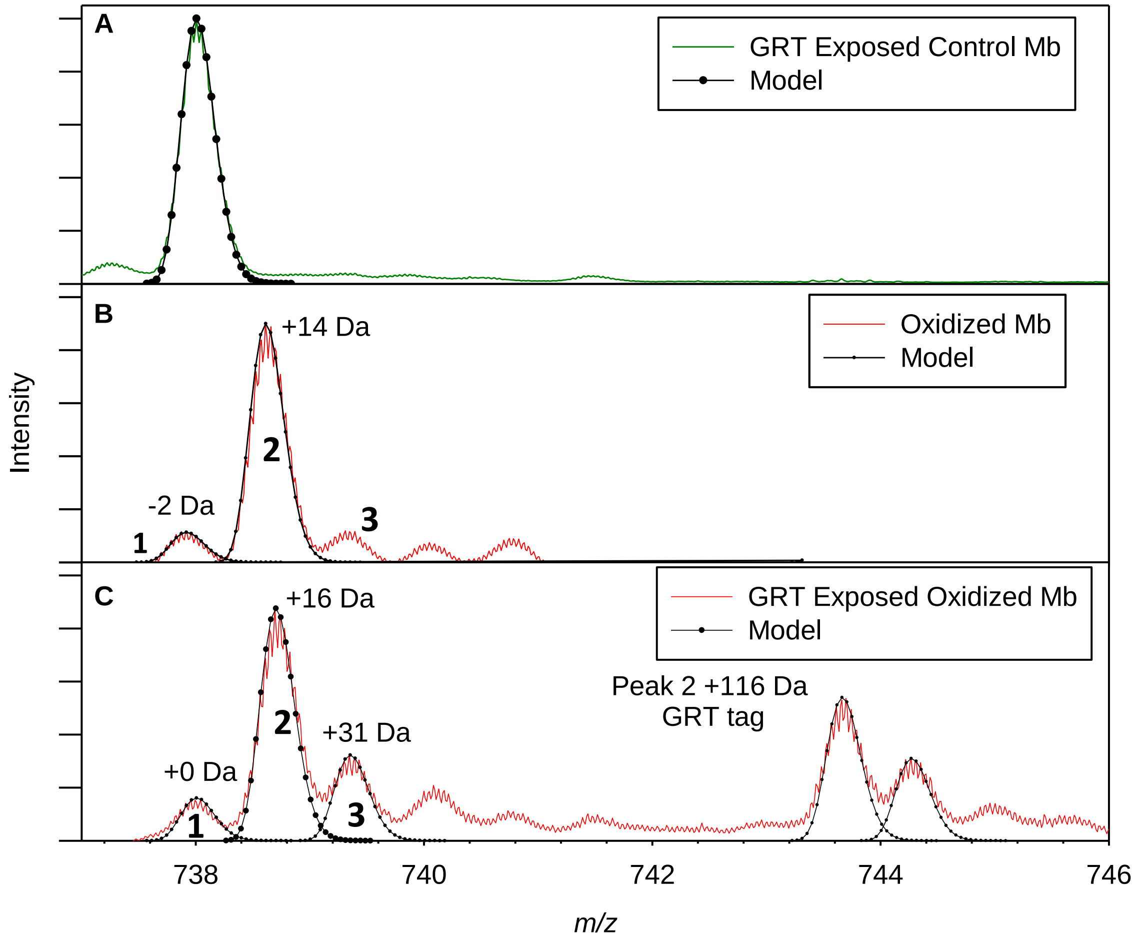

Figure 6: *Mass spectra of Mb, CS 23+, after labeling with Girard's reagent T (GRT). A) Control Mb only shows signals corresponding to the unmodified protein. B) TBHP oxidized Mb, before GRT exposure. C) Mb after exposure to GRT and bond reduction. Two new species are present in panel C, arising from the presence of a carbonyl group after TBHP exposure by the addition of a GRT group (+114 Da GRT, +2 Da bond reduction). Peaks 1 and 2, previously -2 Da and +14 Da respectively relative to control have both shifted +2 Da to the right, indicating the tagging of oxidized Lys by GRT.*

2.3.4 Characterization of Oxidized Mb by Top-Down CID-IM/MS

When proteolytic activity is compromised, as is the case for the scenario encountered here, the efficiency of bottom-up methods is limited. By combining bottom-up and top-down workflows and datasets, better characterization and even residue level resolution can be ascertained. Top-down CID-IM/MS goes beyond conventional MS/MS workflows by using ion mobility to separate fragments created by CID, adding another dimension of analysis and increasing effective resolution. Both control and oxidized myoglobin (Peak 2) samples were analyzed by CID-IM/MS and the resultant fragments were isotopically modelled (Figure 7). Direct comparison of *b* and *y* fragment ions originating from unmodified Mb and from the oxidized protein then reveals mass shifts that are diagnostic of specific covalent modifications.

The first key finding from the data set were multiple unmodified fragments: y28-25, y23 and y22. This observation confirms the previously established finding (chapter 2.3.2) that M131 shows no oxidation and is not the primarily oxidized residue in Peak 2. The second major finding was the region of overlap encompassing fragments: b68, 69, 71 and y83-81. Each of the *b* ions show only a -1 Da shift relative to control while each of the *y* ions in this segment show a +15 Da overall shift. This finding localizes a single lysine oxidation between residues V10 and V68. Although prior depletion of the tryptic peptide 51-56 alludes to oxidation at lysine 56, without further assessment, the specific residue cannot be concluded. The +15 Da shift on the latter end of the protein indicates presence of both a +16 Da oxidation and a -1 Da oxidation.

Initially, the top-down CID-IMS experiments only localized modifications between residues G73 – I112. However, after repeating these experiments with GRT-labelled oxidized protein, the emergence of an unmodified y51 ion permitted localization of additional modifications. By covalently binding lysine and possessing an intrinsic charge, GRT changes both the dissociation energy and pathway, leading to increased fragmentation in the region proximal to the tag.[51] Prior bottom-up MS experiments concluded that K102, K96 and K56 were suspected of -1 Da oxidation, while a +16 Da modification occurred at a site between residues 97-118. Combining all available information from bottom-up and top-down, the lysine oxidation is most likely to be occurring at K102, supported by the induced fragmentation pattern by GRT, and observed tryptic peptide drop-out. Furthermore, the +16 Da modification is localized to residues 96-103, of which Y103 lies closest to heme and has the highest propensity of oxidation via the TBHP MCO.

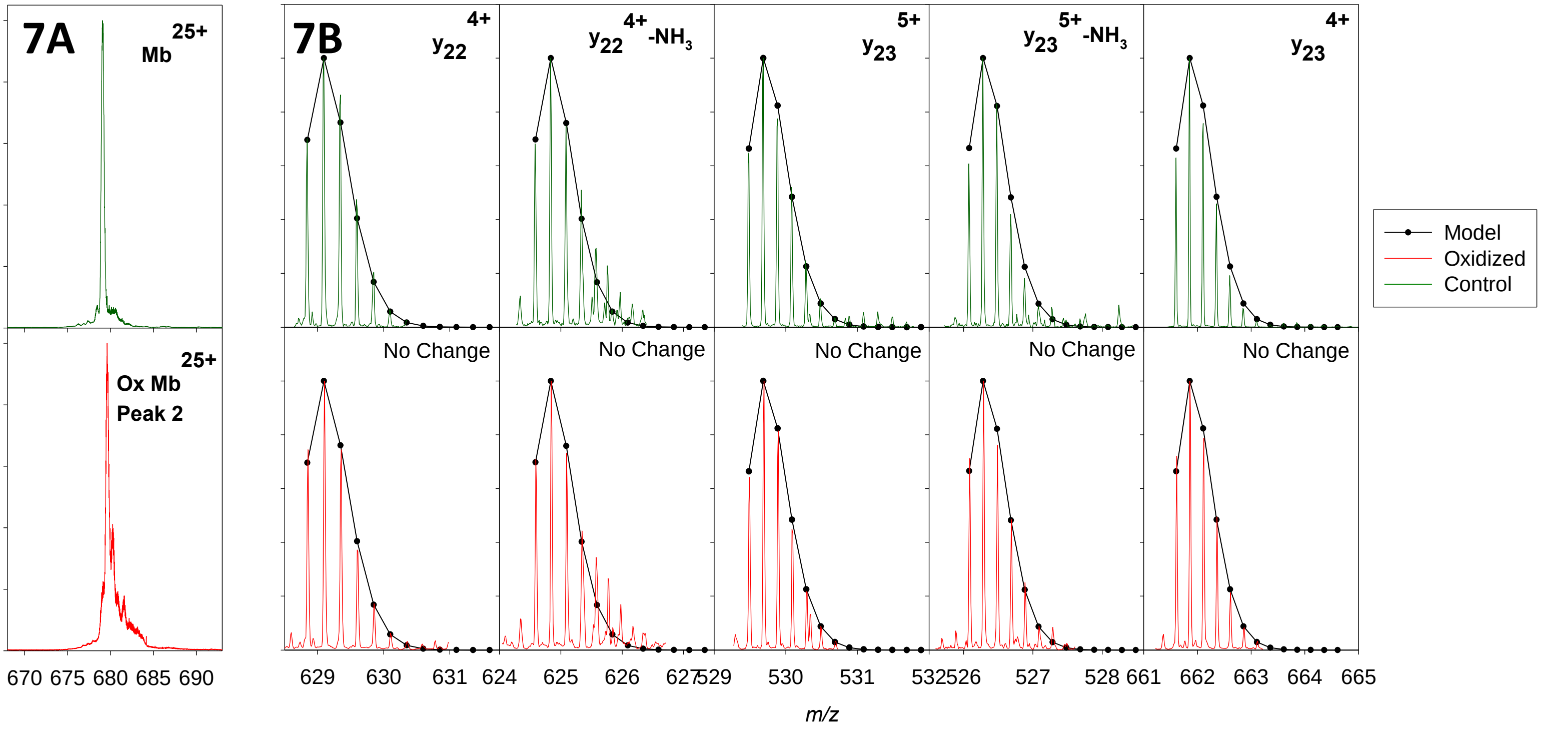

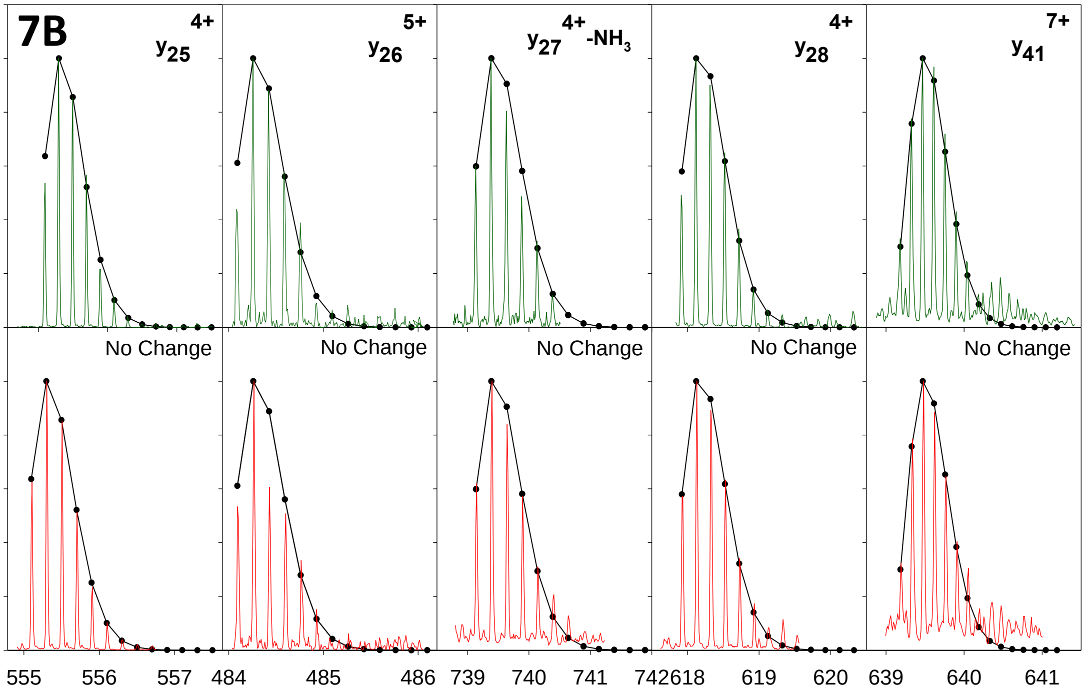

7B

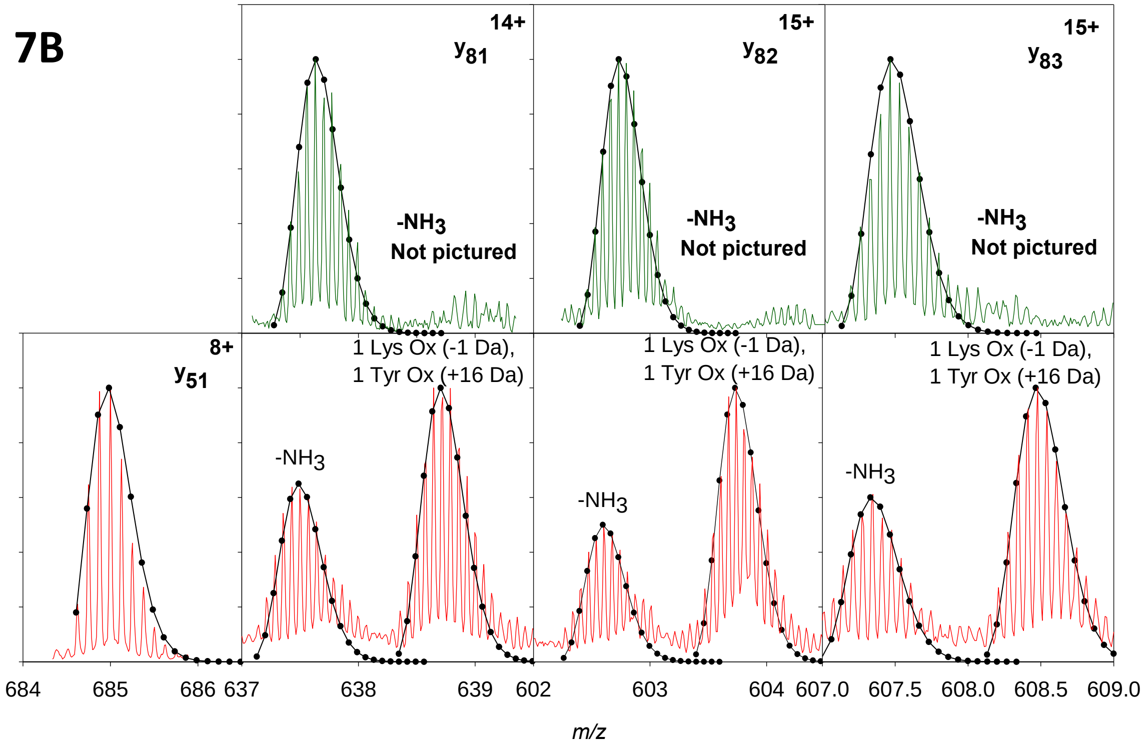
14+
y_{81}
-NH_3
Not pictured
15+
y_{82}
-NH_3
Not pictured
15+
y_{83}
-NH_3
Not pictured
8+
y_{51}
1 Lys Ox (-1 Da),
1 Tyr Ox (+16 Da)
-NH_3
1 Lys Ox (-1 Da),
1 Tyr Ox (+16 Da)
-NH_3
1 Lys Ox (-1 Da),
1 Tyr Ox (+16 Da)
-NH_3
684
685
686
637
638
639
602
603
604
607.0
607.5
608.0
608.5
609.0
m/z

7B

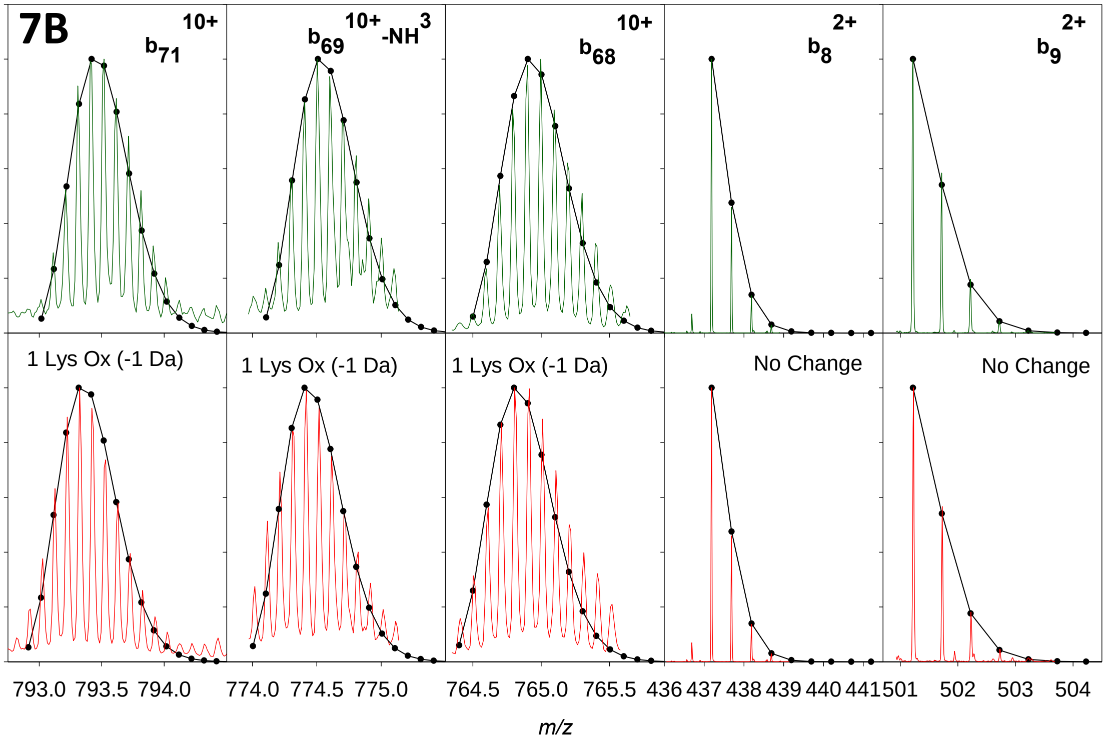
10+
b_{71}
10+
b_{69}
-NH_3
10+
b_{68}
2+
b_8
2+
b_9
1 Lys Ox (-1 Da)
1 Lys Ox (-1 Da)
1 Lys Ox (-1 Da)
No Change
No Change
793.0
793.5
794.0
774.0
774.5
775.0
764.5
765.0
765.5
436
437
438
439
440
441
501
502
503
504
m/z

7C

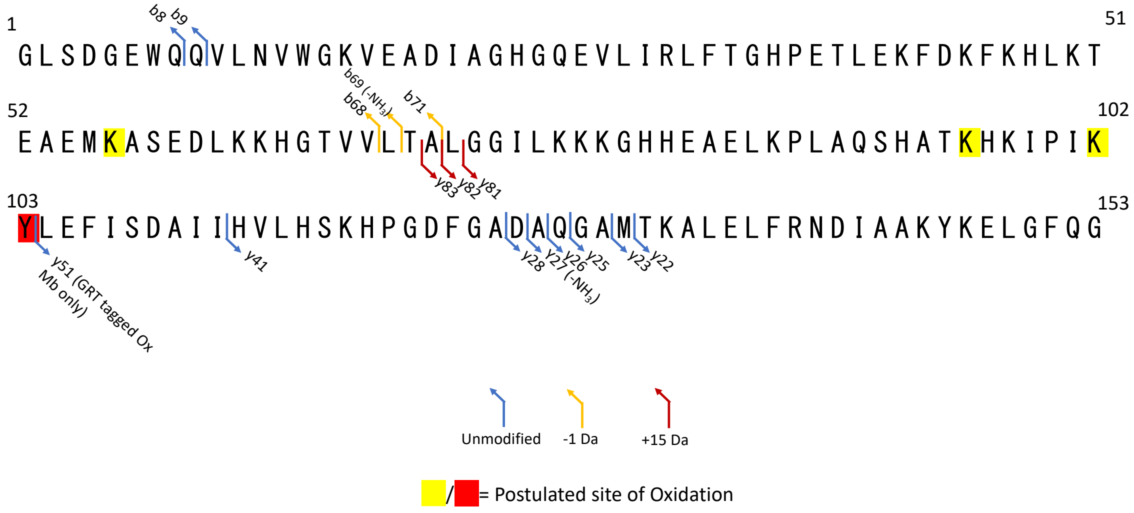
1
51
GLSDGEWQQVLNVWGKVEADIAGHGQEVLIRLFTGHPETLEKFDKFKHLKT
b8
b9
52
102
EAEMKASEDLKKHGTVVLTALGGILKKKGHHEAELKPLAQSHATKHKIPIK
b69 (-NH$_3$)
b68
b71
y83
y82
y81
103
153
YLEFISDAIIHVLHSKHPGDFGADAQGAMTKALELFRNDIAAKYKELGFQG
y51 (GRT tagged Ox Mb only)
y41
y28
y27 (-NH$_3$)
y26
y25
y23
y22
Unmodified
-1 Da
+15 Da
🟨/🟥 = Postulated site of Oxidation

Figure 7: *A) Precursor ion selection of control and oxidized Mb, both CS 25+. B) A series of modelled top down fragments obtained by CID-IM-MS. C) Resultant fragment map, annotated over the Mb sequence.*

2.3.5 Analysis of Protein Dynamics by HDX-MS

After characterization and localization of TBHP-induced oxidative modifications in Mb, our focus shifted to protein dynamics in order to achieve a better understanding of how oxidative damage affects the protein behavior.

As outlined earlier, HDX-MS of oxidized proteins presents a level of complexity that makes this type of experiment difficult, resulting in a scarcity of previous studies on this topic in literature. For addressing these difficulties, the current work involved extra steps to ensure proper characterization of covalent modification and also minimize variability of the sample (i.e., reproducibly achieve complete oxidation while avoiding overoxidation). HDX-MS software results for oxidized protein were manually scrutinized to assure accuracy of identified fragments and chemical shifts. Protease inhibition by oxidative modification again prevented analysis of oxidized peptides. To attain comprehensive coverage in regions where covalent modifications were previously identified, traces of residual unmodified peptides were used after rigorous vetting.

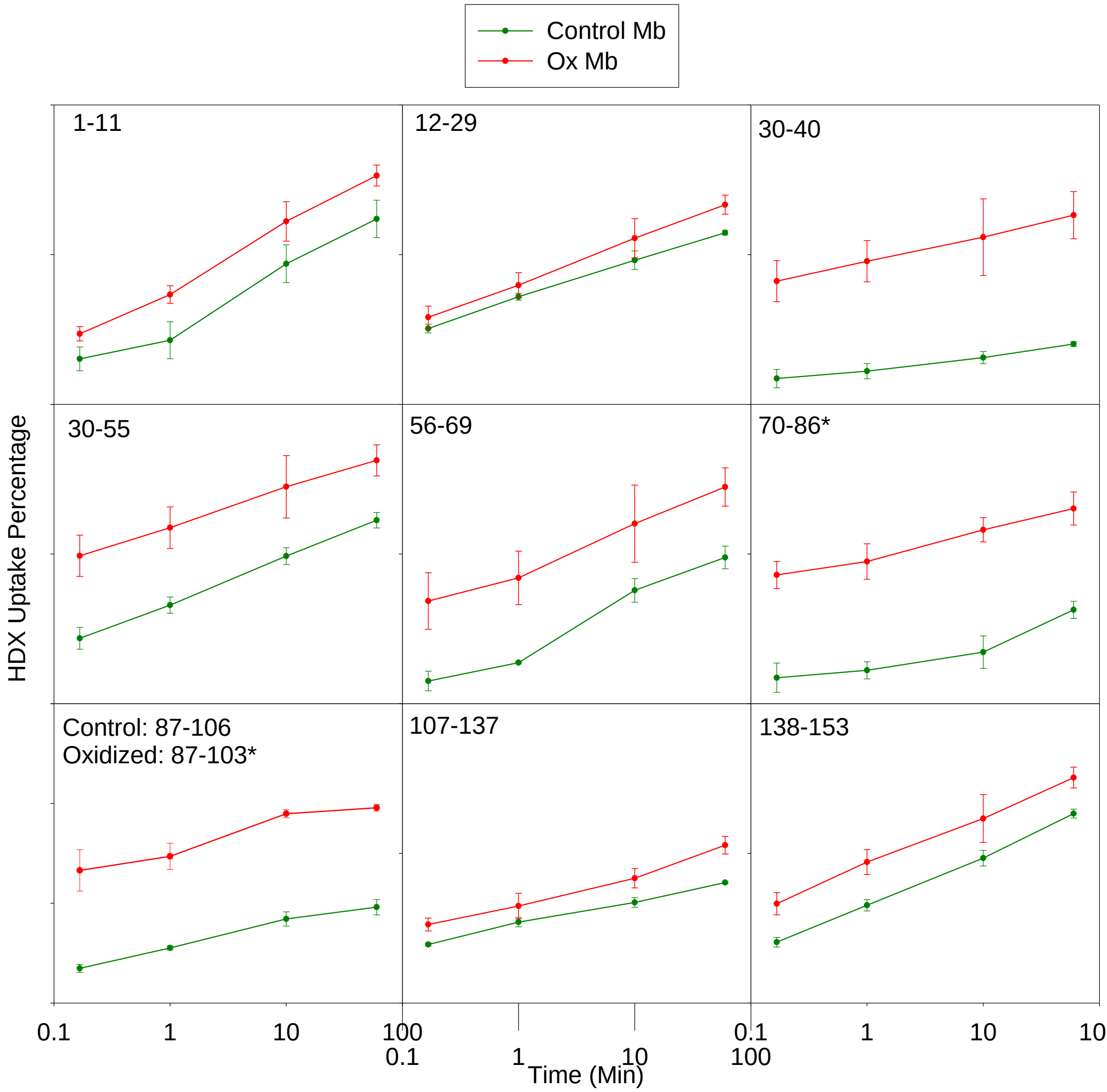

Figure 8: *HDX kinetics of Mb peptic peptides, for unmodified control samples (green) and after TBHP oxidation (red). All points and error bars are derived from 3 replicates. Peptides marked with an asterisk (*) have 2 replicates for oxidized Mb.*

Figure 8 highlights the dynamic differences induced by oxidative stress. All peptides analyzed from an oxidized protein sample showed a higher deuterium uptake relative to the control counterpart. In other words, our data indicates enhanced structural dynamics throughout the protein after oxidation as new intra and intermolecular interactions form as a result of modified side chains. Covalent modifications may also interrupt or destabilize certain intramolecular interactions, producing more labile regions. Regions spatially adjacent to oxidative modifications exhibited the most pronounced uptake differences, visible by the deep red colour projected onto the protein structure in Figure 9. The most affected regions correspond to peptides 30-40 and 87-103/106 (the 87-106 peptide was only present in the control sample, so the 87-103 peptide is substituted for the modified sample). Peptides 30-40 and 30-55 lie directly below K102 and Y103, two proposed sites of oxidation. The large increase in uptake of this region can be attributed to the presence of modified residues. Similarly, peptide 87-103 contains oxidized residues K102 and Y103, possibly inducing partial unfolding, resultant in the high deuterium uptake in this region. Containing the proximal His93, if this peptide is destabilized by the presence of oxidative damage, binding and interaction with heme may be adversely affected. Covalent modifications may also be altering adjacent peptide 70-86, as this region possesses a notable difference between extent of deuteration in control and modified samples.

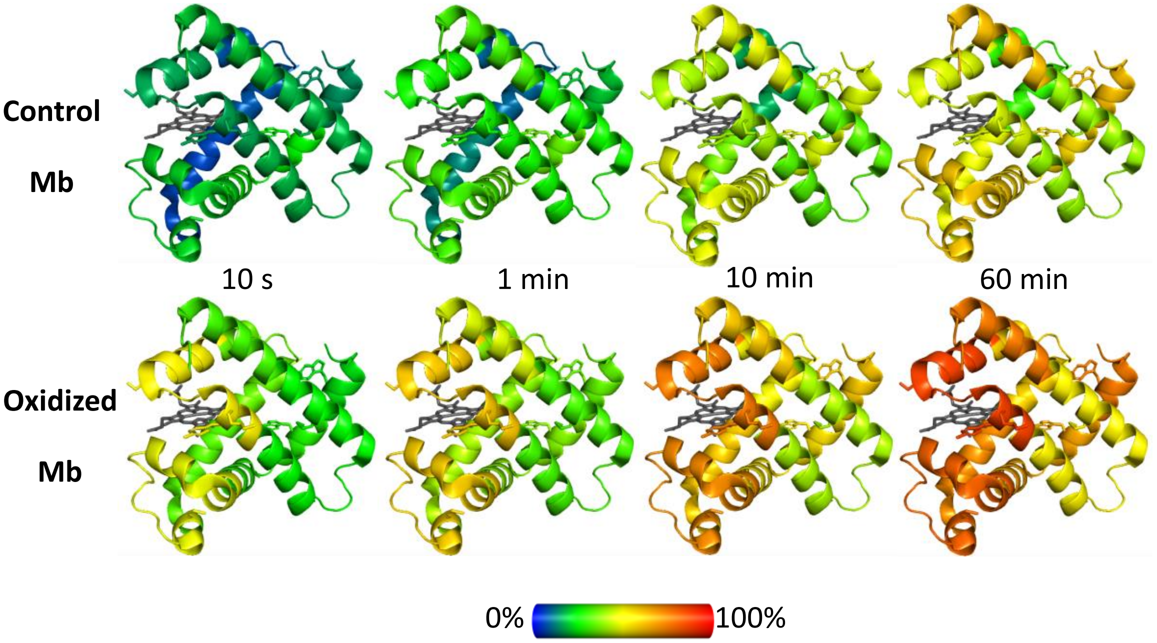

Figure 9: *Graphic representation of HDX kinetics (from Figure 8).*

2.3.6 Oxidation Effects on the Behavior of Electrosprayed Mb Ions in the Gas Phase

Under gentle experimental conditions, (e.g., temperature, solvent, pH, collision energy) electrosprayed proteins in the gas phase can maintain solution-like, non-denatured conformation. In the native state, a protein is fully folded and functional. Upon oxidation, the protein loses its native status, as these modifications may promote unfolding or disrupt intramolecular interactions. Therefore, analysis of gaseous protein ions in this context can divulge critical information about the detriment of oxidative stress on conformational dynamics.

The first stage of gas-phase protein analysis involved the assessing the influence of oxidative damage on folding of the protein using IM-MS (Figure 10). The CCS was measured for the native 9+ charge state of control Mb, as well as Peaks 1, 2, and 3 of oxidized Mb. The first measurement was performed under very gentle conditions (i.e., no collision energy) to obtain a baseline reading. The collision energy was then gradually increased to assess how the different protein species begin to dynamically unfold in reaction as a result of higher energy collision with background gas. Since covalent modification can alter steric and electrostatic interactions, protein structure can either be destabilized and easily unfold or adopt new, more stable conformations instead. Control and oxidized species behave relatively similarly until 15 V of trap collision energy, where all peaks started to shift to a more unfolded state. 17.5 V appears to be a transition point for the control protein, as it adopts two major conformations – both partially shared with all three oxidized species. At 20 V trap collision energy, the control protein begins a major transition to a largely unfolded state – not shared by Peak 1 and 3 of oxidized protein and only partially shared by Peak 2. As energy continues to increase, no large changes are observed in Peaks 1 and 3; however, the control has mainly adopted the state with higher CCS. Peak 2 shares most conformation with Peak 1 and 3, maintaining a small subspecies that echoes that of the control. These findings suggest that the induction of oxidative stress on Mb affects its ability to unfold under native conditions, potentially limiting the dynamic freedom in some domains of the protein.

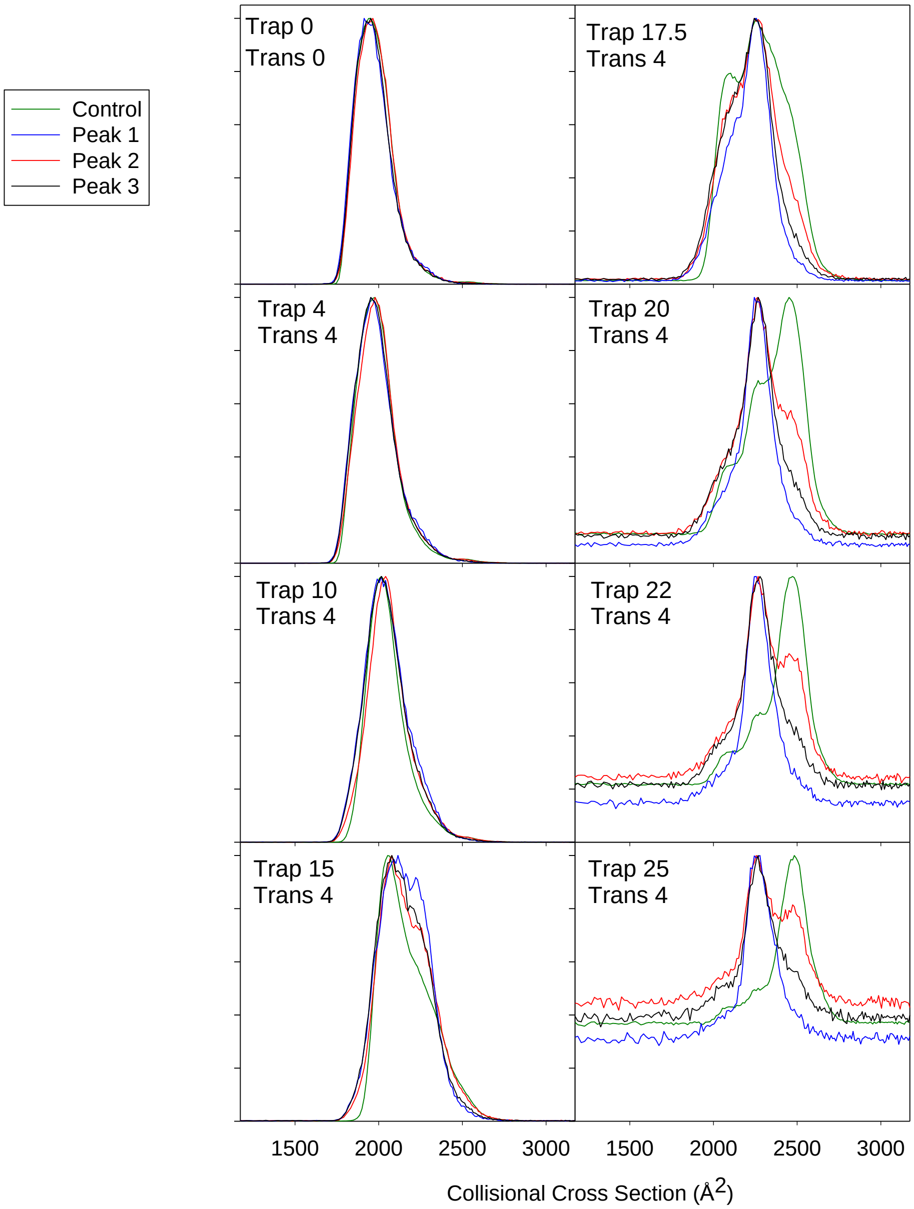

Figure 10: *Unmodified control and oxidized Mb (Peaks 1, 2, 3) were collisionally activated by raising the trap collision energy, and changes in CCS were evaluated by IM-MS. The energy increase caused gradual unfolding of the holo-protein.*

Under gentle ESI conditions, unmodified control myoglobin remained bound to its heme prosthetic group (Figure 11A). A different behavior is seen after TBHP exposure. Figure 11D reveals that upon oxidation, the oxidized protein contains a relatively large fraction of apoMb. This data implies that oxidation events destabilize the protein structure and disrupt coordination of the heme. ApoMb has a higher propensity to unfold than holoMb, and does not retain function.

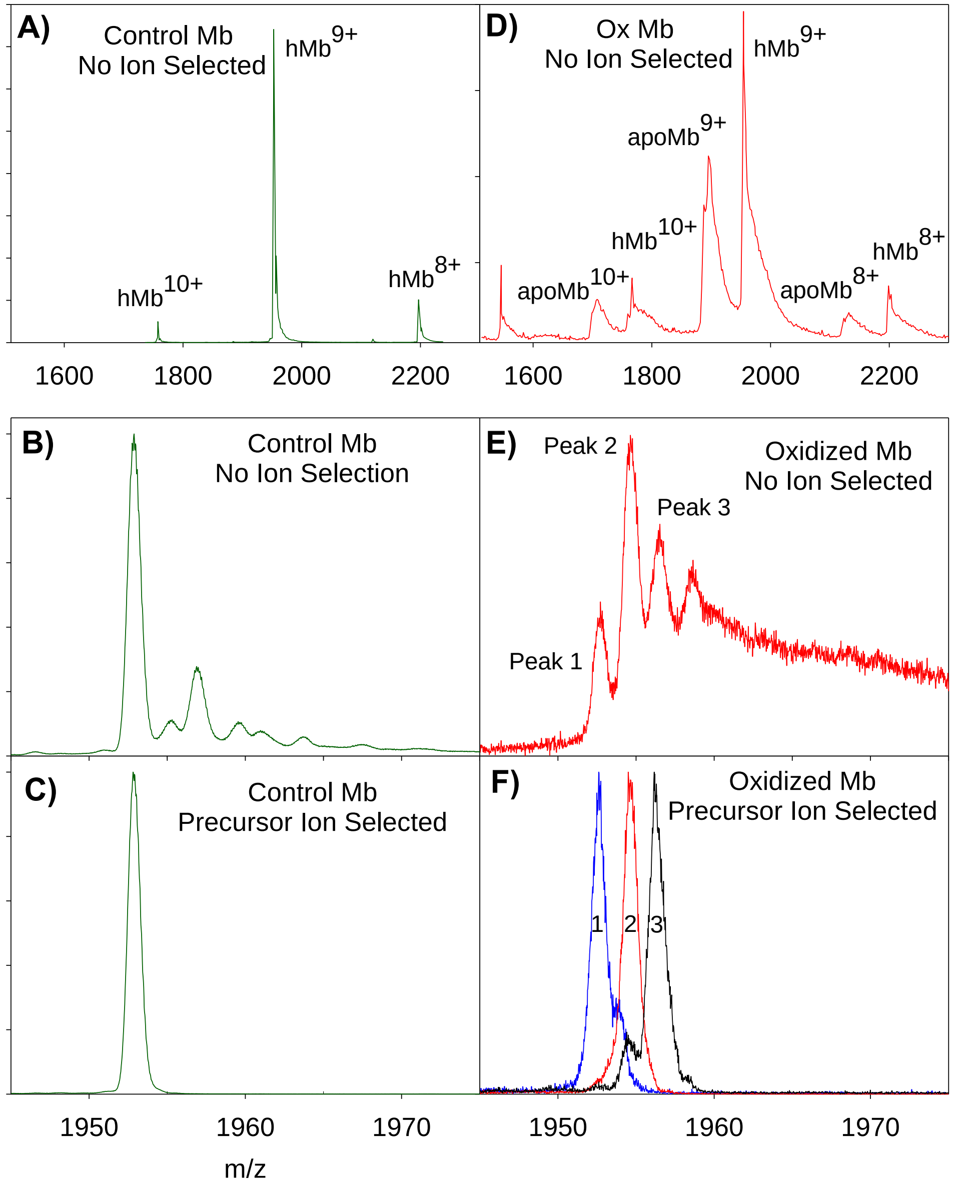

Figure 11: *ESI mass spectra of oxidized (red) and control (green) Mb acquired under non-denaturing conditions. (A, D): Full mass spectra. (B, E): Close-up views of the hMb*$^{9+}$ *signals. (C, F) hMb*$^{9+}$ *signals after precursor selection. The selected ions in panels C and F were then interrogated by collision-induced dissociation (see subsequent figures).*

To further assess the properties of the holo protein, the native 9+ control and Peaks 1, 2, and 3 were selectively subjected to increasing amounts of trap collision energy, inducing dissociation of heme in the gas phase. Figure 12 illustrates this process for control Mb, showing data for only three of the seven collision energy values. This experiment probes the stability of the protein in the gas phase and alludes to its overall stability by measuring propensity to retain heme. On a discontinuous axis (heme on left, *m/z* 616), Figure 12 shows spectra monitoring the production of free heme$^+$ and subsequent apoMb species.

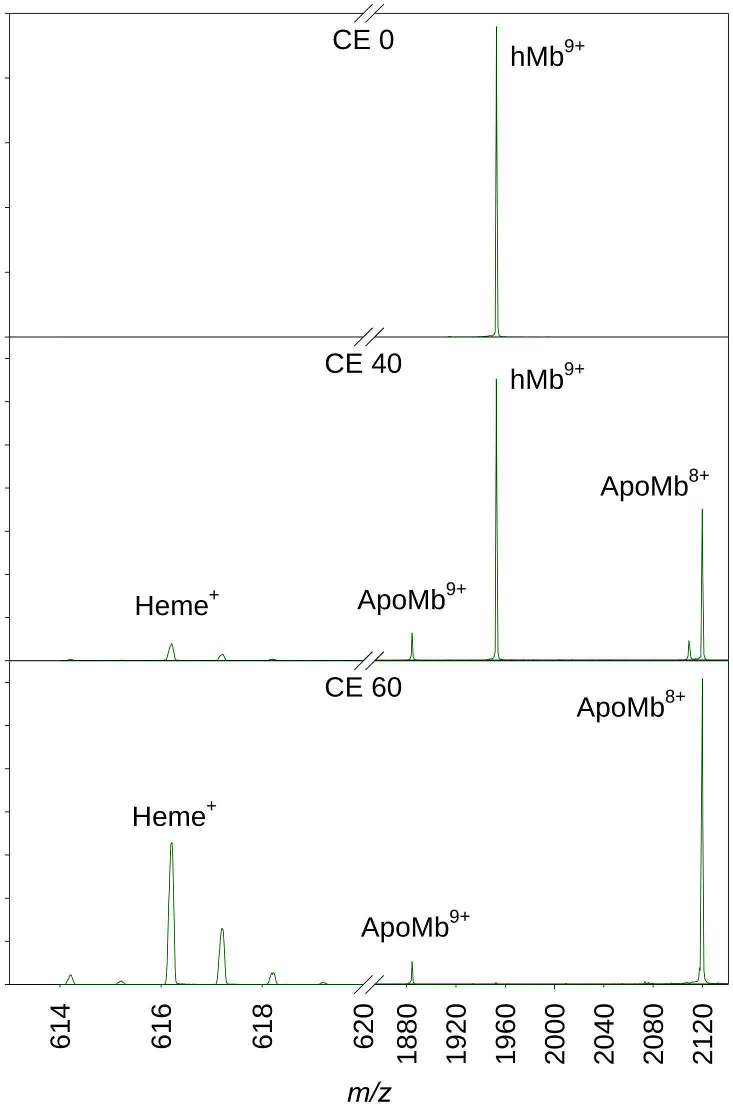

Figure 12: *Collision-induced dissociation of hMb*$^{9+}$*, resulting in the formation of heme*$^{+}$ *and apoMb*$^{8+}$*. A small fraction of the heme leaves as neutral, generating apoMb*$^{9+}$ *product ions. The data shown here illustrate the behavior of an unoxidized control protein sample.*

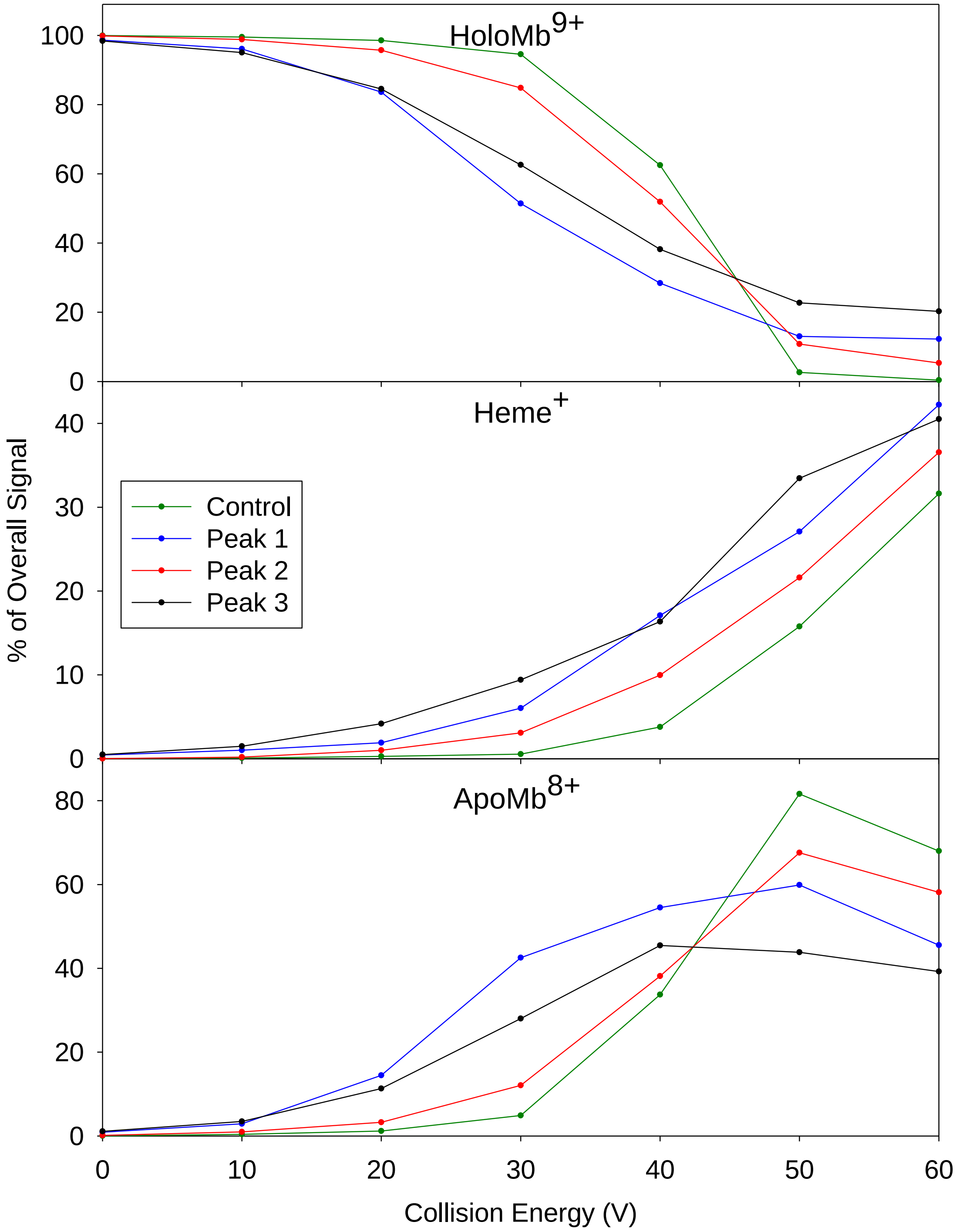

Figure 13: *Collision induced dissociation of hMb^{9+} ions into heme^{+} and apoMb^{8+} the gas phase, unmodified control and after TBHP oxidation (Peaks 1,2,3). Relative percentage of overall signal of heme^{+} (top plot), holo^{9+} (middle plot), apo^{8+} (bottom plot) are plotted as a function of collision energy.*

Figure 13 graphically summarizes the spectral analysis of the experiment depicted in Figure 12 - interrogation of the main peaks: heme, hMb^{9+} and $apoMb^{8+}$. These graphs show the change in proportion of overall signal for heme, hMb^{9+}, and $apoMb^{8+}$ as collision energy increases. Peaks 1 and 3 start losing their heme already at relatively low levels of activation, while control Mb lags behind, releasing heme less readily than the oxidized counterparts. As the collision energy increases, Peaks 1 and 3 most readily deplete the holo 9+ protein, producing apo 8+. Control Mb; however, shows stability through lower collisional energies and resists the transition until higher energy (50 V) where it rapidly converts from holo 9+ to apo 8+. Control Mb exhibits the lowest propensity to release heme, maintaining higher levels hMb instead of early conversion to apoMb like Peaks 1 and 3. These results show that unoxidized Mb exhibits the greatest gas phase stability, while oxidized protein species release heme readily even at low collision energy. These data suggest that the interrogation of gaseous protein ions can yield structural and stability information that is relevant to the behavior of proteins in solution – thereby expanding the MS toolbox.

2.4 Conclusions

MS provides many different methods for analysis of oxidative modification of protein. Alone, each individual method may be insufficient, but upon combining information from the various approaches, a comprehensive picture can be obtained. This data is required for characterizing covalent modifications and assessing their impact on protein structure and dynamics. In the context of myoglobin oxidation, TBHP proved to be an effective agent for obtaining fully oxidized samples. Unlike the previous studies by Imiołek *et al.*,[25] and Keck[24] however, our results clearly demonstrate that TBHP is by no means methionine specific. One main oxidized species dominates while possessing two prominent subsidiaries. Often overlooked in prior works, lysine carbonylation to aminoadipic semialdehyde exists in each of the oxidized species, primarily at K102. The current work was unable to specifically localize the second lysine oxidation with a high degree of confidence; however, it provides a narrow range of possible residues. Careful examination of multiple data sets revealed that Y103 is the predominant site of +16 Da oxidation, contributing to the main oxidized species (Peak 2). HDX-MS required strenuous sample and procedural optimization but provided valuable insight to oxidized protein dynamics. Regions spatially adjacent to sites of oxidative modification exhibited higher deuterium uptake, correlating with high mobility and regional unfolding. The high lability of the 87-103 peptide indicates possible disruption of the His93-heme coordination. Oxidized Mb exhibits higher propensity to unfold and lose its heme, although IMS data show that it adopts a more compact activated structure, relative to its control counterpart. The combination of reproducible oxidation and various MS analysis methods used provides a comprehensive workflow for analyzing effects of oxidative stress on proteins, also highlighting areas of analysis that require closer attention.

2.5 References

1 B. S. Berlett and E. R. Stadtman, *J. Biol. Chem.*, 1997, 272, 20313–20316.

2 W. E. Balch, R. I. Morimoto, A. Dillin and J. W. Kelly, *Science*, 2008, **319**, 916–919.

3 A. Höhn, J. König and T. Grune, *J. Proteomics*, 2013, **92**, 132–159.

4 A. G. Madian and F. E. Regnier, *J. Proteome Res.*, 2010, **9**, 3766–3780.

5 P. R. Angelova and A. Y. Abramov, *FEBS Lett.*, 2018, **592**, 692–702.

6 B. Halliwell and M. Whiteman, *Br. J. Pharmacol.*, 2004, **142**, 231–255.

7 I. Verrastro, S. Pasha, K. T. Jensen, A. R. Pitt and C. M. Spickett, *Biomolecules*, 2015, 5, 378–411.

8 H. Mirzaei and F. Regnier, *J. Chromatogr. A*, 2006, **1134**, 122–133.

9 M. Rykaer, B. Svensson, M. J. Davies and P. Hä, *J. Proteome Res.*, 2017, **16**, 3978–3958.

10 M. J. Davies, *Biochim. Biophys. Acta - Proteins Proteomics*, 2005, **1703**, 93–109.

11 I. Dalle-Donne, R. Rossi, D. Giustarini, A. Milzani and R. Colombo, *Clin. Chim. Acta*, 2003, 329, 23–38.

12 X. Li, Z. Li, B. Xie and J. S. Sharp, *J. Am. Soc. Mass Spectrom.*, 2013, **24**, 1767–1776.

13 E. Shacter, *Drug Metab. Rev.*, 2000, **32**, 307–326.

14 A. L. Lehninger, *Biochemistry*, Worth, New York, 2nd ed., 1975.

15 G. A. Petsko and D. Ringe, *Protein Structure and Function*, New Science Press Ltd., London, UK, 2004.

16 M. Karplus and J. A. McCammon, *Ann. Rev. Biochem.*, 1983, **53**, 263–300.

17 L. Konermann, J. Pan and Y. H. Liu, *Chem. Soc. Rev.*, 2011, **40**, 1224–1234.

18 L. Konermann, S. Vahidi and M. A. Sowole, *Anal. Chem.*, 2014, **86**, 213–232.

19 G. F. Pirrone, R. E. Iacob and J. R. Engen, *Anal. Chem.*, 2015, **87**, 99–118.

20 L. Konermann, J. Pan and Y. H. Liu, *Chem. Soc. Rev.*, 2011, **40**, 1224–1234.

21 L. de Lucca Camargo and R. M. Touyz, in *Textbook of Vascular Medicine*, Springer International Publishing, Cham, 2019, pp. 127–136.

22 E. R. Stadtman and R. L. Levine, *Amino Acids*, 2003, **25**, 207–218.

23 M. J. Davies, *Biochem. J.*, 2016, 473, 805–825.

24 R. G. Keck, *Anal. Biochem.*, 1996, **236**, 56–62.

25 M. Imiołek, G. Karunanithy, W.-L. Ng, A. J. Baldwin, V. Gouverneur and B. G. Davis, *J. Am. Chem. Soc.*, 2018, **140**, 1568–1571.

26 R. Hutchins, M. Hutchins and B. Trost, *Comprehensive organic synthesis: Reduction of C=X to CH2 by Wolff-Kishner and Other Hydrazone Methods*, 8th edn., 1991.

27 G. Schneider and G. A. Sprenger, *Enzym. Kinet. Mech.*, 2003, 197–201.

28 Y. Sun, S. Vahidi, M. A. Sowole and L. Konermann, *J. Am. Soc. Mass Spectrom.*, 2016, **27**, 31–40.

29 D. Eliezer, J. Yao, H. J. Dyson and P. E. Wright, *Nat. Struct. Biol.*, 1998, **5**, 148–155.

30 D. Eliezer and P. E. Wright, *J. Mol. Biol.*, 1996, **263**, 531–538.

31 P. A. Jennings and P. E. Wright, *Science (80-.).*, 1993, **262**, 892–896.

32 S. Cavagnero, Y. Thériault, S. S. Narula, H. J. Dyson and P. E. Wright, *Protein Sci.*, 2000, **9**, 186–193.

33 E. E. Scott, E. V Paster and J. S. Olson, *J. Biol. Chem.*, 2000, **275**, 27129–27136.

34 S. V Evans and G. D. Brayer, *J. Mol. Biol.*, 1990, **213**, 885–897.

35 H. Frauenfelder, S. G. Sligar and P. G. Wolynes, *Science (80-.).*, 1991, **254**, 1598–1603.

36 A. Ostermann, R. Waschipky, F. G. Parak and G. U. Nienhaus, *Nature*, 2000, **404**, 205–208.

37 M. Schmidt, K. Nienhaus, R. Pahl, A. Krasselt, S. Anderson, F. Parak, G. U. Nienhaus and V. Srajer, *Proc. Nat. Acad. Sci.*, 2005, **102**, 11704–11709.

38 R. S. Johnson and K. A. Walsh, *Protein Sci.*, 1994, **3**, 2411–2418.

39 R. G. Keck, *Anal. Biochem.*, 1996, **236**, 56–62.

40 T. Matsui, S. Ozaki and Y. Watanabe, *J. Am. Chem. Soc.*, 1999, **121**, 9952–9957.

41 T. Wazawa, A. Matsuoka, G. Tajima, Y. Sugawara, K. Nakamura and K. Shikama, *Biophys. J.*, 1992, **63**, 544–50.

42 V. Yin, G. S. Shaw and L. Konermann, *J. Am. Chem. Soc.*, 2017, **139**, 15701–15709.

43 V. Yin, S. H. Mian and L. Konermann, *Chem. Sci.*, , DOI:10.1039/C8SC03624A.

44 C. Giulivi and K. J. Davies, *J. Biol. Chem.*, 2001, **276**, 24129–36.

45 D. Tew and P. R. Ortiz De Montellano, *J. Biol. Chem.*, 1988, **263**, 17880–17886.

46 A. Bachi, I. Dalle-Donne and A. Scaloni, *Chem. Rev.*, 2013, **113**, 596–698.

47 J. B. Fenn, M. Mann, C. K. Meng, S. F. Wong and C. M. Whitehouse, *Science*

(80), 1989, **246**, 64–71.

48 D. D. Gouveia, A. M. N. Silva, R. Vitorino, M. R. M. Domingues and P. Domingues, *Eur. J. Mass Spectrom.*, 2014, **20**, 271–278.

49 P. Wood, Humana Press, New York, NY, 2017, pp. 229–232.

50 O. H. Wheeler and O. Rosado-Lojo, *Tetrahedron*, 1962, **18**, 477–482.

51 D. A. Polasky, F. Lermyte, M. Nshanian, F. Sobott, P. C. Andrews, J. A. Loo and B. T. Ruotolo, *Anal. Chem*, 2018, **90**, 2756–2764.

52 S. Reeg and T. Grune, *Antioxidants Redox Signal.*, 2015, **23**, 239–255.

53 E. R. Stadtman, *Free Radic. Res.*, 2006, **40**, 1250–1258.

54 R. Tycko, *Protein Sci.*, 2014, **23**, 1528–1539.

55 M. Bucciantini, E. Giannoni, F. Chiti, F. Baroni, L. Formigli, J. Zurdo, N. Taddei, G. Ramponi, C. M. Dobson and M. Stefani, *Nature*, 2002, **416**, 507–511.

56 V. N. Uversky and A. L. Fink, *Protein Rev.*, 2006, 1,2.

57 L. M. Luheshi, D. C. Crowther and C. M. Dobson, *Curr. Op. Chem. Biol.*, 2008, **12**, 25–31.

58 J. X. Pan, J. Han, C. H. Borchers and L. Konermann, *Biochemistry*, 2012, **51**, 3694–3703.

59 R. G. Spiro, *Glycobiology*, 2002, **12**, 43R-56R.

60 E. R. Stadtman, *Protein Oxidation and Aging*, 1992, vol. 257.

61 D. A. Polasky, F. Lermyte, M. Nshanian, F. Sobott, P. C. Andrews, J. A. Loo and B. T. Ruotolo, *Anal. Chem.*, 2018, **90**, 2756–2764.

3 Conclusions and Future Work

3.1 Conclusions

An aging population accentuates the importance of understanding pathology of common ailments. Oxidative damage is a leading cause of cellular disfunction leading to age-related disease.[1–10] This project employed TBHP to oxidize the model protein, myoglobin, to mimic events of protein oxidative damage, *in vitro*. The work in this thesis explores complementary MS methods that can be used to characterize covalent modification by inducing oxidative damage and assesses the ensuing effect on the dynamics of the protein. The study highlights the insufficiencies and common obstacles of traditional bottom-up characterization methods when working with oxidized protein. Inhibition of proteolytic cleavage and an abundance of false positive hits by proteomics software are two of the main factors that plague bottom-up analysis of oxidized proteins. Experimental design should acknowledge these difficulties accordingly before experimenting further or concluding final results. Top-down analyses are less hindered by protein oxidation, providing a more robust avenue for the identification of covalent modifications. The combination of information provided by bottom-up and top-down MS helps achieve residue-level resolution far better than by each method on its own. With that, covalent modifications can be confidently identified and localized before proceeding to analyze protein dynamics.

To comprehensively describe the effects of oxidative damage on protein dynamics, this work applies a variety of methods including IMS, collision-induced activation (unfolding), collision induced dissociation (CID) and HDX-MS. HDX-MS has long been revered in protein dynamic analysis but the significant lack of literature surrounding oxidized proteins highlights the existing challenges of this methodology. HDX-MS experimentation on oxidized proteins holds the potential to disseminate intricate impacts on protein dynamics that lead to protein aggregation and loss of function. This work addresses complications attributed to sample complexity and accurate peptide mapping to draw conclusions surrounding the dynamic behavior of oxidized protein.

This work is intended to highlight the capability of MS in analyzing oxidized protein and assessing oxidative damage. Oxidative damage plays a central role in various disease mechanisms, such that understanding which workflows will produce accurate and reliable results is imperative. Future work can apply the methods used in this project to successfully study proteins of pathological interest related to common ailments. Myoglobin served as a model protein for the current study, but a similar experimental design can be applied to any protein of interest with minor customizations. Gradually increasing the extent of oxidation on protein systems may also uncover aggregation mechanisms and tendencies. As MS continues to evolve, the series of techniques used in this project will continue to provide a comprehensive suite of information.

3.2 Future Work

Lysine oxidation to aminoadipic semialdehyde remains a commonly overlooked covalent modification due to miniscule *m/z* differences relative to control samples. Characterization of these modifications requires instruments with high resolving power and a trained eye. Development of more robust characterization workflows would help better identify these modifications and the interactions they cause. One of the lysine modifications on myoglobin was localized to a small region of amino acids, but we were not able to pinpoint the exact residue even after the application of multiple proteases and top-down workflows. Future work should assess and utilize the effectiveness of covalent labelling with fixed-charge molecules on promotion of better fragmentation in top-down MS.[11]

Currently, no software suite is available to assist in processing results from CID-IM-MS, resulting in very tedious data analysis; however, manual analysis provides thorough, high-confidence conclusions. Time investment could be largely optimized by development of software suites to assist users with targeted spectral assessment; however too much reliance on software to accurately analyze complex protein systems can oversimplify results. Software results must always be rationalized and verified by users to avoid missing pertinent data and drawing misled conclusions, as proven in this work.

HDX-MS was successfully applied to probe the altered dynamics of an oxidized protein system in this work. Future studies are aimed at obtaining better peptide coverage, specifically in regions containing covalent modifications. With coverage of oxidized peptides, the effect of oxidized residues can be probed on neighboring amino acids. This would provide further insight into oxidative damage dynamics which is currently unobtainable due to deficiencies in bottom-up workflows. Mixed protease columns may be considered for future use. Further, with this work demonstrating the merit of HDX-MS on oxidized proteins, more heavily oxidized protein systems with pathological relevance should be assessed by the same metrics.

3.3 References

1 S. Reeg and T. Grune, *Antioxidants Redox Signal.*, 2015, **23**, 239–255.

2 B. S. Berlett and E. R. Stadtman, *J. Biol. Chem.*, 1997, 272, 20313–20316.

3 E. R. Stadtman, *Free Radic. Res.*, 2006, **40**, 1250–1258.

4 R. Tycko, *Protein Sci.*, 2014, **23**, 1528–1539.

5 M. Bucciantini, E. Giannoni, F. Chiti, F. Baroni, L. Formigli, J. Zurdo, N. Taddei, G. Ramponi, C. M. Dobson and M. Stefani, *Nature*, 2002, **416**, 507–511.

6 V. N. Uversky and A. L. Fink, *Protein Rev.*, 2006, 1,2.

7 L. M. Luheshi, D. C. Crowther and C. M. Dobson, *Curr. Op. Chem. Biol.*, 2008, **12**, 25–31.

8 J. X. Pan, J. Han, C. H. Borchers and L. Konermann, *Biochemistry*, 2012, **51**, 3694–3703.

9 R. G. Spiro, *Glycobiology*, 2002, **12**, 43R-56R.

10 E. R. Stadtman, *Protein Oxidation and Aging*, 1992, vol. 257.

11 D. A. Polasky, F. Lermyte, M. Nshanian, F. Sobott, P. C. Andrews, J. A. Loo and B. T. Ruotolo, *Anal. Chem.*, 2018, **90**, 2756–2764.

4 Curriculum Vitae

Vincent Saullo

Education

York University

Spec. Hons. B.Sc. Pharmaceutical and Biological Chemistry | September 2012 – April 2017

- Undergraduate Thesis ***(Demian Ifa)***: Chemical Composition Analysis of Ginger Rhizome (*Zingiber Officinale*) in Sprouted and Unsprouted Samples Using DESI-MS Imaging

University of Western Ontario

M.Sc. Physical/Analytical Chemistry | January 2018 – Present

- Master's Thesis ***(Lars Konermann)***: Analysis of Oxidatively Damaged Proteins by Mass Spectrometry

University of Toronto

Doctor of Pharmacy | September 2019 - Present

Awards and Acknowledgements

- ***Ontario Scholar and Honor Roll*** – 2012
- ***York University Entrance Scholarship*** – 2012
- ***Kappa Sigma Fraternity Tau-Upsilon Chapter Founding Father and Grand Master*** – 2016/2017
- ***Kappa Sigma Fraternity International Recruitment Award*** – 2016/2017
- ***Kappa Sigma Fraternity International Academic Excellence Award*** – Fall 2016 and Winter 2017

- ***York University Dean's Honor List*** – 2017

Experience

University of Western Ontario

Teaching Assistant | January 2018 – Present

- Involvement in running the *Resource Room* extra help sessions for CHEM 1302, preparing students for exams and ensuring a proper understanding of course material
- Laboratory Instructor for CHEM 1302B
- Laboratory Instructor for CHEM 2384B

Conference Presentations

V. A. Saullo, and L. Konermann "Analysis of Oxidatively Damaged Proteins by H/D Exchange Mass Spectrometry" (poster), *American Society for Mass Spectrometry*, **June 2nd – 6th,** Atlanta, GA, United States of America.

Course Work - UWO

	Weight	Grade
CHEM 9544A – Mass Spectrometry	0.50	0.95
CHEM 9494B – Biophysical Chemistry	0.50	0.90
SGPS 9102 – New Venture Creation		*Pass*